Annu. Rev. Astron. Astrophys. 2004. 42:517–48
doi: 10.1146/annurev.astro.42.010803.115226

First published online as a Review in Advance on June 1, 2004

FINE STRUCTURE IN SUNSPOTS

John H. Thomas
Department of Physics and Astronomy and Department of Mechanical Engineering, University of Rochester, Rochester, New York 14627; email: thomas@me.rochester.edu

Nigel O. Weiss
Department of Applied Mathematics and Theoretical Physics, University of Cambridge, Cambridge CB3 0WA, United Kingdom; email: n.o.weiss@damtp.cam.ac.uk

Key Words Sun, magnetic fields, magnetoconvection, MHD, umbral dots, penumbral filaments, Evershed flow

■ **Abstract** Important physical processes on the Sun, and especially in sunspots, occur on spatial scales at or below the limiting resolution of current solar telescopes. Over the past decade, using a number of new techniques, high-resolution observations have begun to reveal the complex thermal and magnetic structure of a sunspot, along with associated flows and oscillations. During this time remarkable advances in computing power have allowed significant progress in our theoretical understanding of the dynamical processes, such as magnetoconvection, taking place within a sunspot. In this review we summarize the latest observational results and theoretical interpretations of the fine structure in sunspots. A number of projects underway to build new solar telescopes or upgrade existing ones, along with several promising new theoretical ideas, ensure that there will be significant advances in sunspot research over the coming decade.

1. INTRODUCTION

The Sun remains the only star on which magnetic features can be observed in detail, and sunspots are the most prominent of these features. The quest for higher resolution in solar astronomy began as soon as spots were first observed through telescopes, almost 400 years ago. The past decade, however, has seen a major breakthrough, not only from space, with the *Transition Region and Coronal Explorer* (TRACE), but also in ground-based observations, with frame selection, image reconstruction, and the advent of adaptive optics. As a result, it is now possible to resolve features that are only $0.1''$ wide (70 km on the Sun), and the fine structures created by magnetoconvective interactions can at last be recognized. Theoretical understanding of these nonlinear processes has also developed rapidly, largely through advances in numerical modeling, facilitated by the availability of ever more powerful computers. This combination of theory with observations is finally

making it possible to understand the detailed mechanisms that are responsible for the visible structure of a sunspot.

Sunspots are dark because they contain strong magnetic fields that inhibit the normal transport of energy by convection at the solar photosphere. A well-developed spot may have a radius of 10,000–20,000 km, with a dark central nucleus (the "umbra"), surrounded by a less dark, filamentary "penumbra." The umbra radiates energy at only 20% of the normal photospheric rate, corresponding to a temperature deficit of 2000 K, whereas the average penumbral intensity is about 75% of that outside the spot (Bray & Loughhead 1964, Thomas & Weiss 1992a, Stix 2002). The magnetic field is almost vertical at the center of the spot (where it has a strength of up to 3500 G, or 0.35 T) but its inclination to the vertical increases with increasing radius, reaching an average value of 70° at the edge of the spot, where the field strength drops to less than 1000 G.

The revolution in observations of fine structure is best illustrated by the remarkable images obtained from the ground with the new Swedish 1-m Solar Telescope on La Palma. Figure 1 shows two such images, of sunspots near the center of the solar disk. The bright granules are convection cells with plumes of hot gas rising at their centers and a network of cooler sinking gas. The umbrae and penumbrae of the sunspots are clearly visible, with slender bright and dark filaments in the latter. There are also some small dark features, which appear as isolated umbrae or "pores," as well as some penumbral patches. The granulation appears irregular in places, owing to the presence of magnetic fields that are confined to the intergranular lanes and that show up as tiny bright points in this image. Thus, magnetic features are present on all scales, posing a range of problems for the theoretician. Figure 2 shows a region near the limb of the Sun, viewed obliquely and showing three-dimensional relief (because the geometrical height of a surface of unit optical depth varies by several hundred kilometers). It has long been known that the umbra of a sunspot is depressed by about 600 km below the normal photosphere. This "Wilson depression" is due to the reduced opacity resulting from the lower gas pressure (because of the greater magnetic pressure) and temperature in the umbra.

In this review we emphasize recent observations that have revealed fine structure in the umbrae and penumbrae of sunspots as well as the theoretical problems that they pose. In particular, we focus on the puzzling structure of the magnetic field in the penumbra and offer some explanations for its origin.

The review is organized as follows: In the next section we summarize the technical developments that have made such observations possible. In Section 3 we review basic theoretical approaches to understanding sunspot structure, with emphasis on the theory and modeling of magnetoconvection. Then, in the next two sections we describe the observed fine structure of the umbra (Section 4) and the penumbra (Section 5) and discuss theoretical interpretations of these features. The discussion of the penumbra covers not only the structure visible in the continuum (as shown in Figure 1) but also the complicated geometry of the magnetic field and the velocities associated with the well-known Evershed outflow. In Section 6

we investigate the origin of penumbral filaments and argue that magnetic flux is pumped downward by the turbulent convection immediately outside the sunspot. In the concluding section we present a brief summary and look ahead to future observational and theoretical advances.

The reader should be aware that this review does not cover all research on sunspots, but only that dealing with their fine structure. A recent comprehensive review of sunspots has been given by Solanki (2003). Those seeking a broad background in sunspot research are referred to the treatise by Bray & Loughhead (1964) and the volumes edited by Cram & Thomas (1981), Thomas & Weiss (1992a), and Schmieder, del Toro Iniesta & Vázquez (1997). Various aspects of fine structure in sunspots have recently been reviewed by Socas-Navarro (2003) and Bellot Rubio (2003).

2. ADVANCES IN HIGH-RESOLUTION OBSERVING CAPABILITIES

Although our main purpose is to discuss the results of high-resolution observations of sunspots and their theoretical interpretation, it is appropriate that we first discuss some of the remarkable technical advances that have made these observations possible. In this section we briefly review current and planned telescopes, instrumentation, and techniques for high-resolution solar observations. More complete coverage of these topics can be found, for example, in the proceedings of two recent conferences (Rimmele, Balasubramaniam & Radick 1999, Pevtsov & Uitenbroek 2003).

2.1. High-Resolution Solar Telescopes

It has become clear that solar observations with an angular resolution of order $0.1''$ or better are needed to answer many important questions in solar physics (Thomas 1999). This is especially true of sunspots. These observations involve high resolution in the broadest sense, including spatial, temporal, and spectral resolution, requirements that can only be met by a large-aperture, highly efficient solar telescope. Ideally such an instrument would be flown in space, but cost considerations favor ground-based telescopes that compensate for atmospheric seeing with adaptive optics.

Here we describe a few existing and planned solar telescopes that are especially suited for high-resolution observations of sunspots. Further details on these and other solar observing facilities can be found in the comprehensive summary by Fleck & Keller (2003) and in chapter 3 of the book by Stix (2002).

2.1.1. GROUND-BASED TELESCOPES The leading telescope for high-resolution solar observations is currently the Swedish 1-m Solar Telescope (Scharmer et al. 1999), which replaced the Swedish Vacuum Solar Telescope (SVST) on La Palma in May 2002. With its 97-cm aperture and adaptive optics, this telescope produces

diffraction-limited, 0.1″-resolution images of sunspots in the visible (e.g., Figure 1). Although observations at this new facility were initially limited to broad-band and narrow-band imaging, capabilities for spectroscopy and polarimetry are now in place. Several results from this new telescope are described in later sections of this review.

Another major high-resolution facility is the 76-cm Dunn Solar Telescope (DST) at the U.S. National Solar Observatory (NSO) site on Sacramento Peak, New Mexico. With its recently upgraded adaptive optics system, the DST is now producing its best images ever (see Figure 3). The McMath-Pierce Solar Telescope at NSO/Kitt Peak, still the world's largest at 1.5-m aperture, is particularly well suited for observations in the infrared. Other solar telescopes producing high-resolution observations include the French-Italian THEMIS Telescope (90 cm), the German Vacuum Tower Telescope (70 cm), and the Gregory-Coudé Telescope (45 cm) on Tenerife; the Big Bear Solar Telescope (65 cm) in California; and the Dutch Open Telescope (45 cm) on La Palma.

A few projects to build new solar telescopes with apertures larger than 1 m are under way. The 1.5-m German GREGOR telescope replaces the Gregory-Coudé telescope on Tenerife. It is of open-air design, which is less costly than an evacuated or helium-filled design, but nevertheless is very effective in reducing local seeing aberrations, as shown by the success of the Dutch Open Telescope (45 cm).

The most ambitious project is the 4-m Advanced Technology Solar Telescope (ATST; Rimmele et al. 2003), now undergoing design studies at the NSO. The jump to such a large aperture is driven by the fact that high-resolution observations are often limited by the photon flux, not the diffraction limit (Keller 1999, 2003, Thomas 1999). (The number of photons per second per resolution element at the diffraction limit is independent of aperture size, and smaller features evolve more rapidly, requiring shorter exposure times.) The ATST will be an off-axis Gregorian telescope with a short focal-length (f/2) primary mirror. Like the GREGOR telescope, it is of open-air design. The location of the ATST is yet to be determined, pending the results of site testing at six potential sites.

2.1.2. OBSERVATIONS FROM SPACE Although there are no existing or planned large-aperture (1 m or larger) solar telescopes in space, there are missions that provide long, uninterrupted time series or important observations in wavelength bands inaccessible from the ground. The *Solar and Heliospheric Observatory* (SOHO) satellite, in operation since 1996, provides images and spectra in wavelength bands from the ultraviolet to soft X rays. Its location at the Lagrangian L1 point gives it an uninterrupted view of the Sun, making it particularly well suited for helioseismology. The Michelson Doppler Imager (MDI) aboard SOHO provides velocity measurements with angular resolution of 1.3″ and detects p-modes of harmonic degree up to 4500, sufficient for local helioseismology of sunspots. NASA's planned *Solar Dynamics Observatory* will carry an instrument for helioseismological and vector magnetograph observations of the full solar disk at 1″ resolution, to carry on the important work done by the MDI on SOHO.

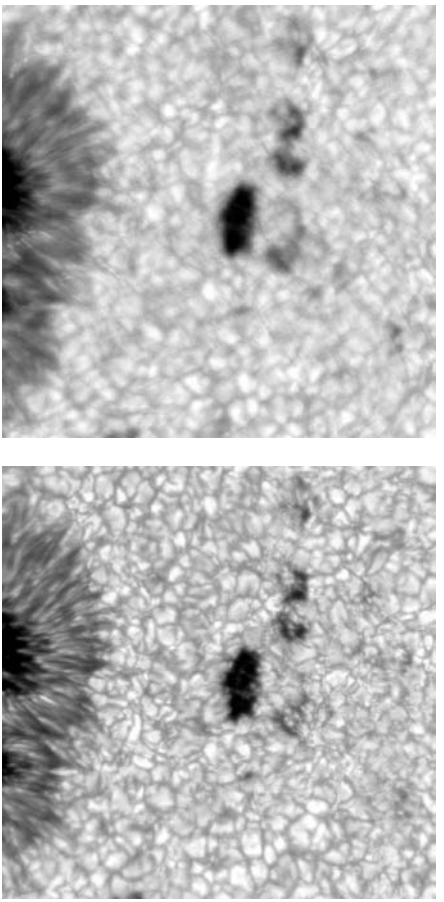

Figure 3 Images of a sunspot taken with the Dunn Solar Telescope (DST) with its adaptive optics system off and on. This AO system often allows the telescope to achieve its diffraction-limited resolution (0.12″ at a wavelength of 430 nm) for periods of up to several tens of seconds, permitting the long exposures required by precision spectroscopic or polarimetric measurements (Rimmele 2004). Without the AO system, such exposures are limited to a resolution of about 1″ during periods of good seeing at this site (courtesy of T. Rimmele, NSO).

TRACE, launched in April 1998, has been providing the highest resolution images ever obtained of the Sun's outer atmosphere, in several wavelength bands from 28 to 250 nm (temperatures from 6000 to 10^6 K). With its aperture of 30 cm, TRACE produces images with angular resolution better than 1″ over its field of view of 8.5′ by 8.5′. TRACE has revealed the remarkable structure of the coronal magnetic field, including the fields associated with sunspots in images such as that shown in Figure 4.

The *Solar-B* mission (Antiochos et al. 1997), a Japanese mission with U.K. and U.S. participation, will carry a 50-cm solar optical telescope for high-resolution imaging polarimetry of the photosphere and chromosphere. Its spectropolarimeter will measure the vector magnetic field in sunspots with resolution near the diffraction limit (about 150 km on the Sun). *Solar-B* is scheduled for launch in 2005. In the context of future space observations, we also mention the *SUNRISE* project to fly a balloon-borne 1-m solar telescope to obtain high-resolution spectropolarimetric observations in the visible and UV (Solanki et al. 2003).

2.2. Instrumentation and Techniques

2.2.1. CORRECTING FOR ATMOSPHERIC SEEING For ground-based solar telescopes, atmospheric seeing is usually the limiting factor in achieving high resolution. Three methods of correcting for seeing are in current use: frame selection, post-processing image reconstruction, and adaptive optics. In some cases, all three techniques are used in the same observational program.

Even during average seeing conditions there are often brief moments of excellent seeing during which nearly diffraction-limited images can be obtained. To take advantage of this, automated frame-selection methods have been developed, in which many short exposures are made at a rapid rate but only the best frames are selected and stored, based on some criterion for image quality (such as maximum rms contrast) that can be implemented on a computer in real time.

The simplest method of post-processing image reconstruction is deconvolution using a modulation transfer function computed for an idealized model of the telescope-detector system. More sophisticated methods correct for seeing using either speckle interferometry or phase diversity. In speckle interferometry, small details beyond the seeing limit are recovered from the speckle pattern in several sequential, short-exposure images. For the Sun, an extended object with no available point source, it is necessary to measure the Fourier phase as well as amplitude. Most solar speckle imaging is based on the method of Knox & Thompson (1974) in which the autocorrelation of the image transform (or cross spectrum) is computed as an average over a large number of short-exposure images. Extensions of this method involve the use of various speckle masks based on the computed triple correlation, or bispectrum.

In the basic method of phase-diversity imaging, two images are recorded simultaneously with the aid of a beam splitter: a conventional focused image and a "diversity" image intentionally defocused by a known amount. These images are both influenced by the same unknown aberrations. The point-spread functions of the two images differ, however, because the phase of the complex wave field in the diversity image is altered (diversified) by a known amount. This then permits a simultaneous solution of the two image convolutions to obtain an object function (the undistorted image) and an aberration function that are consistent with the two images. The method can be generalized to include more than two simultaneous images and different techniques for diversifying the phase. Because the field of

view of the detector is usually larger than the isoplanatic patch, the reconstruction must be applied separately to small segments of the full image, each segment being about the size of the isoplanatic patch (typically a few arcseconds in the visible). Hybrid methods that combine the methods of speckle and phase diversity are also in use (e.g., Paxman, Seldin & Keller 1999).

The most effective method of correcting for seeing, however, is to make the corrections in real time using adaptive optics (AO). The most elementary form of AO employs a single tip-tilt mirror to correct for the lowest-order mode of distortion, a time-varying change in overall inclination of the wavefronts. Such image-motion compensators are often called "active optics," to distinguish them from full AO systems with deformable mirrors that compensate for higher-order distortions of the wavefronts. Early active-optics systems relied on a distinct feature such as a pore to detect image motions, but the development of correlation trackers enabled guiding on the granulation pattern (von der Lühe 1983).

The use of full AO on a solar telescope is challenging because of the lack of a point source to sense wavefront distortions. Instead, the system must rely on the low-contrast, extended source provided by the granulation pattern. Several different approaches, such as curvature sensing and phase diversity, have been pursued. The standard technique of wave-front sensing is the Shack-Hartmann method, in which an image of the entrance pupil is formed on an array of lenslets, each subimage being slightly displaced because of the local tilt of the wave front. These displacements are measured (usually by correlation tracking) and used to control the active mirror.

The first successful application of AO to solar observations was achieved with a 19-segment mirror at the DST (Acton & Smithson 1992). The first regularly operating solar AO system, installed at the DST in 1998 (Rimmele & Radick 1998), used a 24-subaperture Shack-Hartmann wavefront sensor and corrected for the first 20 Zernike modes of wave-front deformation. This system was recently replaced by a high-order system developed jointly by NSO and Big Bear Solar Observatory. Figure 3 shows the typical image improvement produced by this system. An early AO system was installed at the SVST in 1999 and was replaced by a 35-actuator system in 2002 as part of the upgrade to 1-m aperture. Other AO systems are currently under development for THEMIS and the German Vacuum Tower Telescope on Tenerife.

2.2.2. POLARIMETRY High-resolution magnetograms and Dopplergrams obtained with optical filters provide important information on sunspot fine structure (e.g., Title et al. 1993; Rimmele 1995a,b), and more efficient filters employing multiple-etalon Fabry-Perot interferometers (e.g., Tritschler, Schmidt & Rimmele 2002) will enhance this approach. To determine the full vector magnetic field in a sunspot, however, we need measurements of the full polarization state of the light, as determined by the four Stokes parameters I, Q, U, and V (Stenflo 1994, Sigwarth 2001). Polarimetric measurements are also useful in minimizing the persistent problem of stray light. For example, velocity measurements based on the Doppler

shift in Stokes *V* are largely uncontaminated by stray light from the nonmagnetic photosphere.

Because of the relatively long exposure times required, polarimetric measurements are especially susceptible to atmospheric seeing. Hence, polarimeters designed specifically to take advantage of an AO system, such as the Diffraction-Limited Spectropolarimeter (Lites et al. 2003) at the DST and the Tenerife Infrared Polarimeter (Martínez Pillet et al. 1999), will lead the way in resolving the fine structure of the magnetic field in sunspots.

2.2.3. INVERSION METHODS Measurements of the spectrum and polarization state of solar light must be transformed into information about the distribution of temperature, velocity, and magnetic field in the solar atmosphere. These transformations take several forms, including direct determination of Doppler shifts within a spectral line profile, forward modeling employing spectral synthesis, and techniques that invert the equations of radiative transfer. Especially important for sunspots are techniques for inversion of the Stokes parameters to determine the vector magnetic field. All of these transformations involve the assumption of some physical model for the solar atmosphere, and this model dependence is often the largest source of uncertainty in the interpretation of high-resolution observations.

The theoretical basis for the inversion methods are the transfer equations for polarized radiation, applied to a model atmosphere. A nonuniform magnetic field within a resolution element produces abnormal Stokes profiles with more than two lobes. The simplest model that can reproduce these profiles involves two different magneto-atmospheric components existing side by side within the resolution element. In a typical inversion method of this type, the Stokes profiles are calculated for a two-component atmosphere, consisting of a magnetic part and a nonmagnetic part. (Within a sunspot, the nonmagnetic component can simply represent stray light from the surrounding nonmagnetic photosphere.) The computed synthetic Stokes profiles are fitted iteratively to observed profiles using response functions and an algorithm that minimizes some "merit" function defining the goodness of fit, through variations in a set of free parameters such as field strength, field inclination, line-of-sight velocity, and filling factor of the magnetic component. Another approach is based on a single atmospheric component with vertical gradients (Westendorp Plaza et al. 2001). Increased computing power has enabled the use of more sophisticated inversion techniques involving more realistic model atmospheres. Inversion methods for high-resolution solar data are discussed in several recent reviews (del Toro Iniesta & Ruiz Cobo 1996, Socas-Navarro 2001, Bellot Rubio 2003, del Toro Iniesta 2003).

3. THEORETICAL BACKGROUND

Sunspots are the proving ground for magnetohydrodynamic theory under astrophysical conditions. Nowhere else in astrophysics is this theory confronted with such a wealth of detailed observations. But significant progress is being made in

theoretical work, especially in numerical simulations that are beginning to reproduce some of the fine structure and dynamics in sunspots. In this section we review some of the basic magnetohydrodynamic theory related to sunspots. Specific theoretical models of particular sunspot features are discussed along with the relevant observations in Sections 4 to 6.

3.1. Axisymmetric Magnetostatic Sunspot Models

The simplest models of a pore or a sunspot are axisymmetric, with a meridional (poloidal) magnetic field confined to a flux tube that is bounded by an azimuthal current sheet. Because the ambient atmosphere is stratified, with pressure dropping nearly exponentially with height, the field has to fan out upward in order to maintain a pressure balance at the boundary. The rate at which energy emerges from the sunspot is reduced not only by the expanding geometry of the field, but also by magnetic suppression of convection (see Jahn 1992, 1997). In a highly conducting plasma, magnetic field lines tend to move with the fluid, and are therefore distorted by transverse convective motion; the Lorentz force (which results from tension along the field lines) resists this distortion and therefore inhibits convection. The superadiabatic gradient within the flux tube therefore increases until an equilibrium is reached, and the spot appears cooler and darker than its surroundings.

Although energy transport is predominantly by radiation at the visible surface of the umbra, convection must take over just below, for it is impossible to construct a purely radiative sunspot model (Schlüter & Temesváry 1958). Models can, for instance, be constructed by calculating an atmosphere with a reduced mixing length (to simulate magnetic suppression of convection) and assuming a potential field within the flux tube. That leaves the position of the azimuthal current sheet on the outer surface of the flux tube to be determined as a free boundary problem, which can be solved as an integral equation (Schmidt 1991).

It is not possible, however, to maintain a lateral pressure balance between the umbra, which is lower than the normal photosphere, and the field-free plasma outside the spot if the poloidal field is force-free. Thus it becomes necessary to include azimuthal volume currents in the penumbra. To avoid this awkward situation, Jahn & Schmidt (1994) introduced two current sheets, one at the outer boundary of the flux tube (the magnetopause) and the other at the interface between the penumbra and the umbra. They also assumed that some of the energy radiated from the penumbra is supplied by convective processes that transfer energy across the magnetopause where the flux tube tapers inward with depth below the photosphere. The resulting family of models, parametrized by their total magnetic flux, provides a plausible representation of the global structure of sunspots below the solar surface. For a large spot with a flux of 2×10^{22} Mx (200 TWb) the radius of the magnetopause drops smoothly from 20 Mm at the surface to 12 Mm at a depth of 5 Mm and then to 9 Mm at 10 Mm depth. This corresponds to a fourfold decrease in the cross-sectional area of the flux tube, with a corresponding increase in field strength. As we have mentioned, however, there are large fluctuations about the azimuthally averaged structure in any real sunspot.

3.2. Modeling Nonlinear Magnetoconvection

To investigate these fluctuations it is necessary to model the interactions between turbulent convection and magnetic fields in an electrically conducting plasma. Indeed, sunspots provided the original motivation for studying magnetoconvection, which has developed into a significant topic in its own right and is covered in a number of reviews (e.g., Proctor 1992, Schüssler 2001, Weiss 2002). Much of the earlier work was restricted to incompressible fluids (in the Boussinesq approximation), but the main qualitative results hold for compressible fluids as well. In the absence of any dissipative processes a fluid layer is unstable when it is superadiabatically stratified, but if thermal conductivity and viscosity are included then the superadiabatic gradient has to exceed some critical value. Moreover, magnetic fields inhibit the onset of convection and so this critical value increases when a magnetic field is imposed. Furthermore, the nature of convection depends critically on the ratio, ζ, of the magnetic to the thermal diffusivity (which is typically small in a star). If ζ is large, convection sets in as steady overturning motion, but if ζ is small and the field is sufficiently strong, convection appears as oscillations that correspond to trapped, thermally excited magnetoacoustic waves. Also, the stronger the field the higher the horizontal wavenumber of the initial perturbation, and therefore in the umbra of a sunspot we might expect to see oscillatory motion in very slender cells.

Once the critical superadiabatic gradient is exceeded, convection is limited by nonlinear effects. Although there is a weakly nonlinear (or mildly superadiabatic) regime that can be tackled analytically, it soon becomes necessary to rely on computation. The availability of high-performance computers has revolutionized such calculations. There are two different approaches. Vigorous nonlinear behavior can be explored systematically in idealized models that make it possible to isolate the various processes that are involved. Alternatively, all those processes can be included in an attempt to simulate the real solar atmosphere.

3.2.1. IDEALIZED NUMERICAL EXPERIMENTS The development of turbulent three-dimensional magnetoconvection has been studied systematically in idealized configurations both for a Boussinesq fluid (Cattaneo, Emonet & Weiss 2003) and for a strongly stratified perfect gas (Rucklidge et al. 2000, Weiss, Proctor & Brownjohn 2002). In order to establish how patterns of motion evolve, it is essential to solve the relevant equations in a domain that is much wider than the individual cells that form. Thus, progress has depended on access to ever more powerful computers.

Figure 5 shows some results of numerical experiments on compressible convection in a strong vertical magnetic field (Weiss, Proctor & Brownjohn 2002). Because the diffusivity ratio ζ is proportional to the density, it increases with depth in a stratified layer. (This mimics the effects of ionization below the solar photosphere.) In this case, oscillatory convection is favored locally at the top of the layer, where $\zeta < 1$, whereas overturning convection is favored at the bottom, where $\zeta > 1$. The nonlinear solution in the upper panel of Figure 5 takes

the form of spatially modulated oscillations: there is an irregular array of rising plumes at fixed positions, and the plumes wax and wane aperiodically in amplitude. Magnetic fields are swept aside by the plumes as they impinge upon the upper boundary, and hence magnetic flux is concentrated into a network that encloses the plumes. The solution in the lower panel of Figure 5, for exactly the same parameter values (but different initial conditions), shows an entirely different pattern. There is a tight cluster of broad and vigorously convecting plumes from which magnetic flux has been expelled; these plumes are surrounded by a region with stronger fields and weak, small-scale convection. This phenomenon of flux separation appears to be robust. As the imposed field is further reduced, flux-separated solutions become the only stable state until the field is globally so weak that magnetic flux is concentrated between the mesocellular features into narrow lanes, where the fields are locally intense (as in the facular regions shown in the upper panel of Figure 2). Thus, there is a transition from small-scale convection (initially steady but then time-dependent) to flux separation and then to intermittent magnetic fields as the mean field strength is reduced. In the limit as the imposed field becomes extremely small there is also the possibility that a turbulent field can be maintained by small-scale dynamo action (Cattaneo 1999, Vögler & Schüssler 2003).

3.2.2. CONVECTION IN AN INCLINED FIELD As long as the imposed magnetic field is vertical, no horizontal direction is preferred and the convection pattern can be stationary. This degeneracy is removed when the field is inclined, and the tilt defines a unique horizontal direction. It follows that convection in a stratified layer will set in as a traveling pattern (Matthews et al. 1992). Two-dimensional calculations show that both the form of this pattern and the direction in which it travels depend sensitively on the inclination and strength of the magnetic field, as well as on the degree of nonlinearity (Hurlburt, Matthews & Proctor 1996, Julien, Knobloch & Tobias 2000, 2003).

Three-dimensional behavior is illustrated in Figure 6, based on calculations by Hurlburt, Matthews & Rucklidge (2000). As the inclination of the imposed field to the vertical is increased, there is a transition from spatially modulated oscillations (for a vertical field) to a pattern of cellular oscillations that travels away from the direction of tilt, and then to a traveling, roll-like pattern as the field becomes more nearly horizontal. In the limit when a strong horizontal magnetic field is imposed, it has long been known that convection occurs preferentially in rolls aligned with the field, so that field lines are transported bodily by the motion.

3.2.3. DETAILED SIMULATIONS Convection at the photosphere is dominated by the expansion of broad rising plumes as they impinge upon a layer that is stably stratified. These plumes are enclosed by a network of rapidly sinking fluid, which, at greater depths, is focused into vigorously falling plumes. Detailed simulations, including the effects of ionization and radiative transfer, have been extraordinarily

successful in reproducing the observed properties of the solar atmosphere (Stein & Nordlund 1998). Magnetic fields are swept aside by the expanding plumes and concentrated in the intergranular lanes, to form pores at junctions in the mesogranular network. The lower panel of Figure 2 shows the results of one such simulation, designed to be compared with the companion image from observations.

3.3. Dynamics of Individual Flux Tubes

A different approach to understanding the structure and dynamics of a sunspot has been to study the behavior of an individual magnetic flux tube embedded in an ambient magnetoatmosphere representing the overall sunspot. This approach generally assumes that the flux tube is thin, in the sense that the radius of the tube is much less than both its radius of axial curvature and the local density scale height, and that the flow along the tube is uniform across the cross-section. In the context of sunspots, the thin-flux-tube approach has mostly been aimed at understanding the Evershed flow, both in steady-state flow models (Meyer & Schmidt 1968, Thomas 1988, Degenhardt 1989, Montesinos & Thomas 1997) and in transient-flow models involving transverse motions of the flux tube (Schlichenmaier, Jahn & Schmidt 1998a,b). These models of the Evershed flow are discussed in more detail in Section 5.4. Schlichenmaier (2002) has suggested that the flows in a moving-tube model of the Evershed flow are also responsible for most of the vertical heat transport in the penumbra; this is discussed further in Section 5.3.3.

We add a note of caution about treating the dynamics of individual flux tubes within a sunspot penumbra. There is no conceptual problem with the notion that an individual, isolated magnetic flux tube, bounded by a current sheet, moves within field-free surroundings (as, for example, in models of isolated flux tubes rising through the convection zone). In the case of the sunspot penumbra, however, the surroundings of the individual flux tube are also a strongly magnetized medium, and the discontinuities at the surface of the flux tube thus involve both the strength and the direction of the magnetic field, requiring complex surface currents. In reality, the magnetic field configuration varies smoothly, and it is not clear that an individual flux tube can retain anything like its identity, especially in cases where it undergoes large excursions within those surroundings.

4. UMBRAL FINE STRUCTURE

We now turn to a detailed discussion of the observations and theoretical interpretations of fine structure of a sunspot, beginning here with features in the umbra and continuing in the next section with features in the penumbra. Dividing the discussion between umbral and penumbral features in this way is convenient but not always ideal; for example, some inward-moving penumbral grains penetrate well into the umbra. Fine structure in the umbra has also been reviewed recently by Socas-Navarro (2003).

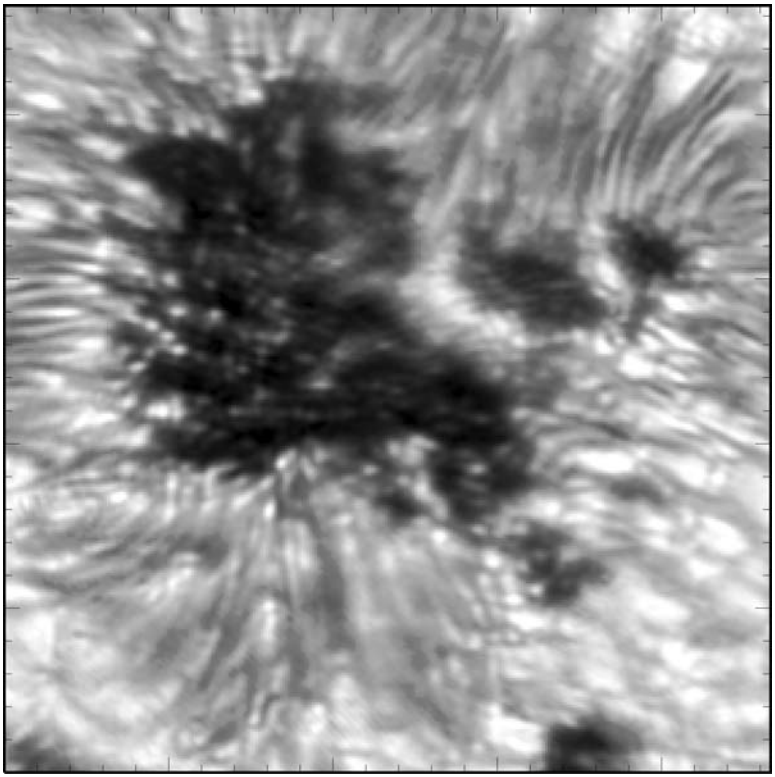

Figure 7 Sunspot image exposed to show umbral dots, indicating convection in the umbra. The image has been corrected using phase-diversity reconstruction. Tick marks are at intervals of 1″ (from Tritschler & Schmidt 2002a).

4.1. Umbral Dots

Umbral dots are small, bright features embedded in the darker umbral background (see Figure 7). They are found in essentially all sunspots and pores. Although earlier observations had shown a granular pattern in the umbra, the smaller-scale umbral dots were first reported by Thiessen (1950) and were rediscovered by Danielson (1964) in Stratoscope observations. Recent high-resolution observations not only reveal many individual umbral dots but also show a diffuse background pattern with intensity varying smoothly with position (Sobotka, Brandt & Simon 1997b).

The reported sizes of umbral dots range from about 0.8″ (580 km) down to the current resolution limit of about 0.2″ (140 km), although the largest dots in this range may well be clusters of smaller dots. The number of umbral dots increases with decreasing size, suggesting that there are many unresolved dots smaller than 0.2″, and the smaller dots are more evenly distributed over the penumbra than the larger ones (Sobotka, Brandt & Simon 1997a, Tritschler & Schmidt 2002b). In

large umbrae there are often dark nuclei, regions almost uniformly dark and free of at least the larger umbral dots. These dark nuclei probably correspond to regions of stronger magnetic field in which convection is severely inhibited (Weiss 2002).

Umbral dots are sometimes divided into two classes: "central" dots found in the inner part of the umbra, and "peripheral" dots located near the umbra-penumbra border (Grossmann-Doerth, Schmidt & Schröter 1986). The peripheral umbral dots are usually brighter than the central ones. The intensity of umbral dots ranges from about 0.2 to 0.7 times the normal photospheric intensity at visible wavelengths. The intensity of the dark umbral background generally increases from the center to the edge of the umbra and also varies locally; the intensity of the umbral dots may be related to this background intensity (Sobotka, Bonet & Vázquez 1993, Denker 1998, Tritschler & Schmidt 2002b).

Early observations generally found that the peripheral umbral dots had inward proper motions whereas the central dots were stationary (e.g., Kitai 1986), but this division has been shown to be not very sharp (Sobotka, Brandt & Simon 1997b). Nevertheless, many of the peripheral umbral dots are penumbral grains that penetrate the umbra and continue to move radially inward (see Section 5). Umbral dots have a wide range of lifetimes, ranging from a few minutes to one hour or more. As spatial resolution has improved, generally shorter lifetimes have been found; for example, Ewell (1992) found lifetimes up to 2 h but a mean lifetime of only 15 min. Sobotka, Brandt & Simon (1997a) also found a wide range of lifetimes; dots with shorter lifetimes are more numerous, and two-thirds of the dots have lifetimes of 10 min or less.

Magnetic field and Doppler velocity measurements of umbral dots pose a considerable challenge, and not surprisingly the results to date are not consistent. Recent observations indicate a reduction of 10–20% in the magnetic field strength in the dots compared to the surrounding umbra (Kneer, Soltau & Wiehr 1990, Pahlke & Wiehr 1990, Wiehr & Degenhardt 1993, Schmidt & Balthasar 1994, Tritschler & Schmidt 1997, Socas-Navarro 2003), although a few observations have shown essentially no weakening of the field in the dots (Zwaan, Brants & Cram 1985, Lites et al. 1991). As Degenhardt & Lites (1993a,b) have pointed out, if the umbral dots are low-lying features, they will appear as intensity enhancements in the continuum but will have very weak signatures slightly higher in the atmosphere where photospheric spectral lines are formed. In this regard, Wiehr & Degenhardt (1993) found a field strength reduction of up to 20% in brighter, peripheral umbral dots in Fe 6843 but little or no reduction in Ca 6103, formed some 350 km higher in the atmosphere.

The various measurements of Doppler velocities in umbral dots are not at all in agreement. Some show no significant motion (Zwaan, Brants & Cram 1985, Schmidt & Balthasar 1994, Wiehr 1994), whereas others show weak upflows with speeds up to 300 m s^{-1} (Lites et al. 1991, Socas-Navarro 2003). Stronger upflows of 1–3 km s^{-1} have also been reported (Kneer 1973, Pahlke & Wiehr 1990). Recently, Hartkorn & Rimmele (2003) found that, whereas the peripheral umbral dots usually show upflows, the majority of the smaller, central umbral dots show weak downflows at speeds up to 300 m s^{-1}.

In summary, the observations of umbral dots show intensity and velocity features over a wide range of length and time scales, with smaller, more rapidly changing features being more numerous. The observations generally suggest a convective origin for the umbral dots, with both stationary and moving patterns of convection present in the umbra. This complicated picture presents a considerable challenge for the theory of magnetoconvection.

4.2. Convection in the Umbra

In a typical spot the strong magnetic field at the center of the umbra is very nearly vertical, and therefore up-down motions are favored. At the solar surface, where radiative transport is efficient while ohmic diffusion is a slower molecular process, the ratio ζ of magnetic to thermal diffusivity is much less than unity, and hence we expect convection to set in as overstable oscillations with slender elongated cells, corresponding to trapped slow magnetoacoustic waves (Cowling 1976). Below the photosphere, however, the radiative diffusivity is drastically reduced, owing to the increase in opacity caused by ionization, with the result that $\zeta > 1$ at depths between 2000 and 20,000 km. A local analysis then indicates that convection should set in as overturning motion. Numerical experiments suggest that this apparent incompatibility is resolved by the appearance of spatially modulated oscillations in the nonlinear regime (Weiss et al. 1990, 1996; Hurlburt, Matthews & Rucklidge 2000; Weiss 2002). Although there is a stationary pattern of rising plumes near the base of the convecting layer, adjacent plumes wax and wane alternately in vigor, in such a way that the velocity at any fixed point in the upper region actually reverses. In a large domain with vigorous convection these oscillations become both spatially and temporally aperiodic, a pattern that can explain the observed properties of umbral dots (Blanchflower, Rucklidge & Weiss 1998, Weiss, Proctor & Brownjohn 2002). Because the umbral photosphere is stably stratified, the underlying pattern of convection is partially obscured (Lites et al. 1991). Only the largest and most vigorous plumes can penetrate this radiative blanket, so the smallest features can barely be detected.

The umbrae of large spots contain dark nuclei that appear almost uniform and free of larger umbral dots. These nuclei may well be examples of flux separation. They contain stronger magnetic fields that restrict convective motion to very slender plumes that scarcely penetrate the radiative blanket, while the weaker fields surrounding the nuclei allow a greater range of scales (Weiss, Proctor & Brownjohn 2002). The apparent inward motion of the brightest umbral dots is most likely a wavelike translation of the convective pattern, which is halted by the stronger, more vertical fields in the dark nuclei.

4.3. Light Bridges

During the lifetime of a sunspot its umbra may be crossed by one or more narrow, bright bands known as "light bridges." Light bridges follow sutures or fissures in the umbra, delineating the individual pores or umbrae that assembled to form the larger umbra or that will later move apart during the decay phase of the sunspot.

Narrow light bridges come and go, but toward the end of a spot's life the umbra is often divided by one or more light bridges that have grown in width and reach photosphere-like conditions, with photospheric intensity and a nearly normal granulation pattern (Vázquez 1973).

Most light bridges are segmented along their length, with bright segments resembling tiny granules separated by narrow dark lanes oriented perpendicular to the axis of the bridge and by a narrow, central dark lane running along the axis of the bridge (Berger & Berdyugina 2003). Not all light bridges exhibit this segmented structure, however; some that extend into the penumbra are unsegmented and resemble more the elongated bright filaments seen in the penumbra (Lites et al. 2004). Light bridges of these two types are shown in Figure 8. This image, taken near the solar limb, gives a perspective view that shows that the segmented light bridge is an elongated, tent-like structure, with the central dark lane being the high point of a ridge elevated above the dark umbral floor (Lites et al. 2004). This height differential can be explained by an increased opacity attributable to the increased temperature, and in part by an increased gas pressure attributable to a reduced magnetic field strength in the bridge.

The magnetic field geometry varies considerably from one light bridge to another, but the field is generally more horizontal than in the surrounding umbra

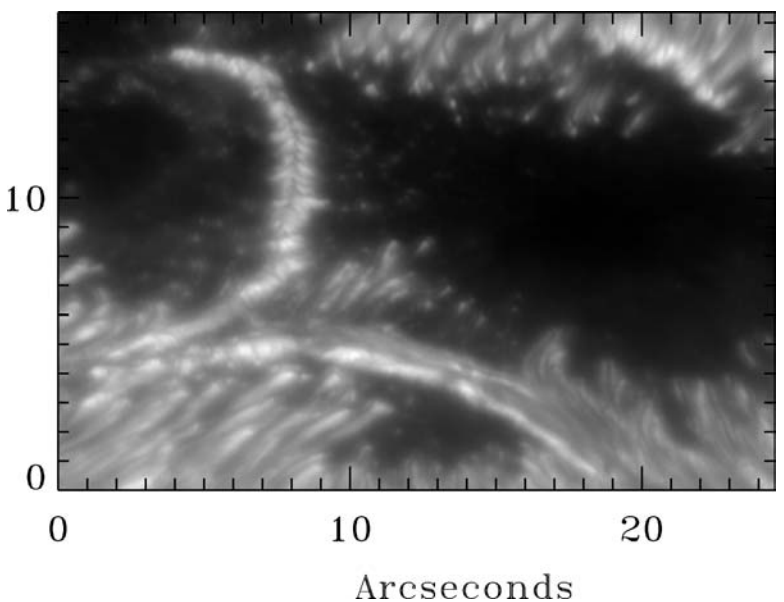

Figure 8 Blue continuum image of two light bridges in a large umbra near the solar limb. The image is oriented with its vertical direction along a solar radius with the closest point on the limb toward the top. In this perspective view, the light bridge at the upper left shows a raised, segmented structure, while the bridge along the bottom shows little segmentation and extends well into the penumbra (from Lites et al. 2004).

(Leka 1997) and in some cases may be locally horizontal, or even of reverse polarity (Lites et al. 2004). The magnetic field strength within the bridge is certainly weaker than that in the nearby umbra and it decreases downward. Indeed, recent observations (Martínez Pillet et al. 2003) are consistent with an essentially field-free region at the deepest visible level but with magnetic canopies spreading from either side of the bridge and merging above the bridge, where the associated intense electric currents heat the base of coronal loops having a footpoint precisely above the light bridge (as seen in TRACE images).

The patterns of motion and intensity in a light bridge are consistent with convection in a narrow slot, with sinking fluid in the axial channel. Moreover, the correlation between vertical velocity and continuum intensity in the larger granules in a light bridge confirms that they have a convective origin (Rimmele 1997). Their time-dependent behavior is certainly consistent with that exhibited by aperiodic spatially modulated oscillations. Nevertheless, it is not possible, in our present state of knowledge, to be sure whether the observed motion in any individual light bridge has a magnetoconvective origin or is caused by convection penetrating from below into an elongated field-free gap.

5. PENUMBRAL FINE STRUCTURE

5.1. Penumbral Filaments and Grains

The distinguishing property of a sunspot is the presence of a penumbra, and the most striking features of penumbral fine structure, easily visible at moderate spatial resolution (1″–2″), are the bright and dark filaments, aligned nearly radially and covering the entire penumbra. The terms "bright" and "dark" here have only local meaning; there are often larger-scale intensity variations within the penumbra, and an individual bright filament can in fact have lower intensity than a dark filament elsewhere.

The width of individual penumbral filaments is near or below the current limit of resolution and hence has been controversial. Earlier studies generally attempted to measure the widths directly from photometric profiles (e.g., Muller 1973b, Bonet, Ponz & Vázquez 1982), but recent studies have attempted more objective measures based on the spatial power spectrum of the penumbral intensity. Sánchez Almeida & Bonet (1998) found a flat power spectrum and concluded that the typical filament width is well below their resolution limit of about 0.2″. Sütterlin (2001), however, found an enhancement of spatial power at around 0.35″ (250 km) and suggested that this was the preferred width of filaments. Observations with the new Swedish 1-m telescope (Rouppe van der Voort et al. 2004), with spatial resolution of 0.12″ (80 km), give a power spectrum that is not flat (it drops off roughly as k^{-4}, where k is the wavenumber), but also shows no distinct peak corresponding to a preferred width. This implies that there are unresolved filaments with widths less than 80 km.

At sub-arcsecond resolution, a bright penumbral filament is generally found to consist of a number of individual features called penumbral grains (Muller

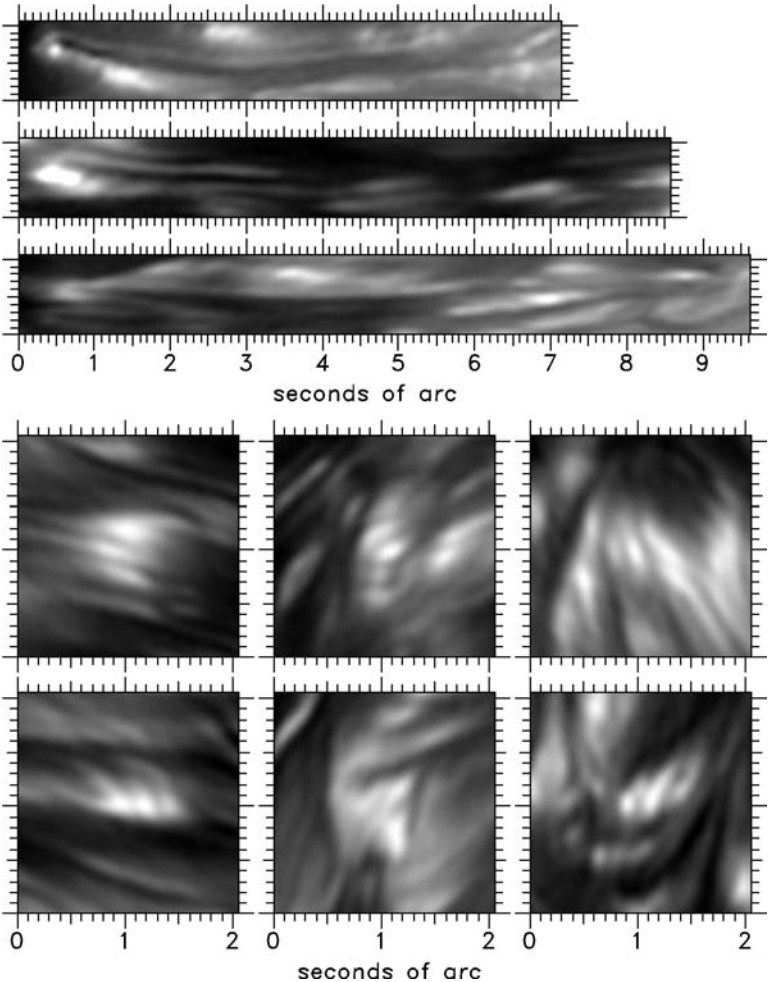

Figure 9 Images of long penumbral filaments and segmented penumbral grains, at nearly 0.1″ resolution, taken with the Swedish 1-m Solar Telescope (from Rouppe van der Voort et al. 2004).

1973a,b). The width of the grains is typically 0.5″ (350 km) or less, and their lengths range from about 0.5″ to 3.5″ (350 to 2500 km). At the highest available resolution (see Figure 9), however, many of the bright filaments are seen to consist of several narrower components, some of which have lengths as great as 5″–9″ (3500 to 6500 km) and thus can not properly be called grains (Rouppe van der Voort et al. 2004). These observations also show that the most grain-like features are generally located at the end of the filaments nearest the umbra, and that these grains have internal structure with a few dark bands crossing them (as shown in

Figure 9). The intensity of the grains ranges from about $0.85 I_{phot}$ to $1.10 I_{phot}$; that is, some of the brightest grains exceed the temperature of the brightest granules outside the sunspot by some 150 K (Tritschler & Schmidt 2002b).

The penumbral grains generally move in the radial direction. Early observations found only inward motion of penumbral grains, but subsequent observations have shown that the motion of the grains is typically inward in the inner penumbra and outward in the outer penumbra (Wang & Zirin 1992, Molowny-Horas 1994, Denker 1998, Sobotka, Brandt & Simon 1999). Roughly speaking, there is a dividing circle located at about 60% of the radial distance from the inner to the outer edge of the penumbra, inside of which the grains move radially inward at speeds of about 0.5 km s^{-1}, and outside of which the grains move outward at about the same speed (Wang & Zirin 1992) or perhaps slightly higher speeds of about 0.75 km s^{-1} (Sobotka & Sütterlin 2001). The inward-moving penumbral grains often penetrate into the umbra (where they become peripheral umbral dots; see Section 3.1) and continue to move inward for a time at speeds of up to 0.5 km s^{-1} (Ewell 1992). Most of the outward-moving grains disappear before reaching the outer boundary of the penumbra, but roughly a third of them cross this boundary and evolve into either a small bright feature (of diameter less than 300 km) or a normal photospheric granule, and continue to move radially outward away from the sunspot (Sobotka et al. 2002).

White-light images of the penumbra averaged over 2–4 h still show filamentary structure (Balthasar et al. 1996, Sobotka, Brandt & Simon 1999), indicating a long-term stability of the magnetic field configuration. The paths of new penumbral grains tend to follow trajectories nearly identical to those of the grains that preceded them at a given location (Sobotka, Brandt & Simon 1999).

Any interpretation of these observations has to answer the following critical questions. What is the nature of the convective processes in the bright and dark filaments? Do the apparent horizontal motions of penumbral grains represent actual displacements of the gas and magnetic field (as, for example, in the moving flux tube model described in Section 5.3.3), or are they generated by a traveling pattern of magnetoconvection in an inclined magnetic field, as outlined in Section 3.2.2? We return to these issues in Section 5.3.1 below.

5.2. Interlocking-Comb Geometry of the Penumbral Magnetic Field

There is an apparent contradiction between the direction of the average magnetic field in the penumbra, which has a strong vertical component, and that of the horizontal Evershed outflow (see Section 5.4 below) because there should be no flow across the field in a highly conducting plasma. It has, however, been known for 35 years that the inclination of the magnetic field in the penumbra varies azimuthally, being more nearly horizontal in the dark filaments (Beckers & Schröter 1969). Yet it is only since 1990 that high-resolution observations have been able to reveal the extraordinary interlocking-comb structure of the magnetic field (Degenhardt

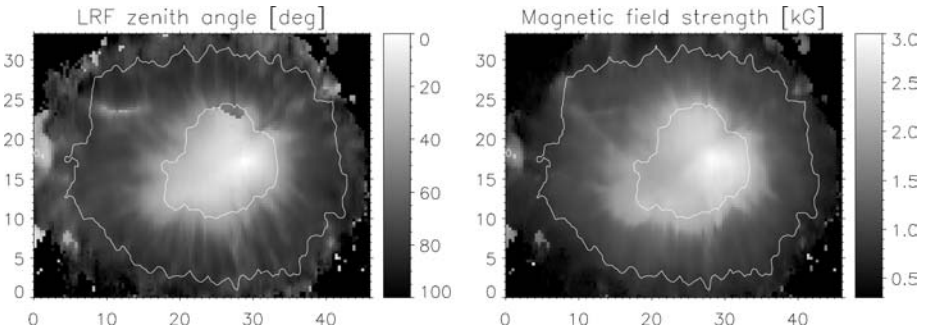

Figure 10 The interlocking-comb geometry of the penumbral magnetic field is shown in these gray-scale plots of the inclination angle (to the vertical in a local reference frame) and strength of the magnetic field in a symmetric sunspot. These quantities are based on an inversion of measured Stokes profiles using a single-component magnetic atmosphere with vertical gradients (adapted from Bellot Rubio 2003).

& Wiehr 1991, Title et al. 1992, 1993, Schmidt et al. 1992, Lites et al. 1993, Solanki & Montavon 1993, Hofmann et al. 1994, Stanchfield, Thomas & Lites 1997, Mathew et al. 2003, Bellot Rubio et al. 2003, Bellot Rubio 2003). This unexpected geometry is perhaps the most remarkable feature of a sunspot's magnetic field. Figure 10 shows the field structure in the penumbra, with its azimuthal variations in field inclination and field strength, as observed at high resolution (Bellot Rubio 2003). The fields in the bright and dark filaments differ in inclination by 30–40°; in the outer penumbra (where the Evershed flow is most prominent) the field in the dark filaments is almost horizontal, whereas that in the bright filaments is inclined at 50–60° to the vertical. At the umbra-penumbra boundary, the inclinations are about 65° and 30°, respectively. Moreover, whereas the fields from dark filaments typically spread into a shallow canopy lying just above the solar surface (or even dive beneath it), loops emerge from bright filaments into the corona and extend over great distances across the Sun, as shown both by X-ray observations (Sams, Golub & Weiss 1992) and by the striking images obtained from TRACE (Winebarger, DeLuca & Golub 2001, Winebarger et al. 2002), such as that shown in Figure 4. It is apparent from these results that the magnetic fields in the bright and dark filaments must be regarded as distinct, because their geometry precludes any significant interchanges between them (Weiss et al. 2004).

This structure has been called by various names: "spines" (the more vertical fields) and "inter-spines" (the more horizontal fields; Lites et al. 1993); "fluted" structure (Title et al. 1993); "uncombed" structure (Solanki & Montavon 1993, Bellot Rubio 2003). Here we use the descriptive term "interlocking-comb" structure (Thomas & Weiss 1992b). The general picture derived from Stokes spectropolarimetry is of a two-component atmosphere (Bellot Rubio 2003). The filling factor for the component containing the more inclined field decreases with increasing height in the atmosphere. These results appear to be compatible either with

a model in which the more horizontal fields are confined to isolated flux tubes, enclosed above and below by the more vertical component (Solanki 2003), or with one in which the more horizontal fields are contained in thin vertical slabs that are bounded above but extend downward to a significant depth (Weiss et al. 2004).

The extraordinary magnetic structure associated with the filamentary penumbra raises a number of theoretical issues but also provides important clues to the formation and maintenance of the penumbra. We address the latter topics in Section 6.

5.3. Convection in the Penumbra

The penumbra, which emits about 95% of the energy radiated from a sunspot, poses a much more serious theoretical challenge than the umbra. The energy that emerges through the umbra can either be carried upward from great depths by convective processes within the underlying flux tube or, more likely, be drawn from the thermal energy of the plasma deep below the spot, at depths where the Kelvin-Helmholtz time is much longer than the period of the solar cycle (Spruit 1992). On the other hand, the energy emitted from the penumbra, to which bright and dark filaments contribute equally (since the latter occupy a greater area), must include a major contribution that is brought in laterally from the surrounding plasma (Jahn & Schmidt 1994, Rucklidge, Schmidt & Weiss 1995). Moreover, it is necessary to relate the underlying pattern of convection to the complex magnetic structure of the penumbra discussed in Section 5.2. This structure implies that there cannot be any significant interchanges between bright and dark penumbral filaments and that the corresponding convective processes have to be considered separately (Weiss et al. 2004).

5.3.1. TRAVELING PATTERNS IN THE BRIGHT FILAMENTS Behavior in the bright filaments can be modeled by considering convection in a narrow slot with an inclined magnetic field. Then we should expect to find a traveling pattern of spatially modulated oscillations, although the direction of travel cannot be predicted. The bright grains would correspond to hot rising plumes, and high-resolution observations (Scharmer et al. 2002) suggest that they also have a double-roll transverse structure, with sinking fluid along the axis of the filament. The apparent proper motion of the grains is best interpreted as a traveling wave, whose direction of propagation depends on the inclination of the field and is inward in the inner penumbra but outward in the outer penumbra where the field is more steeply inclined to the vertical (Hurlburt, Matthews & Rucklidge 2000, Weiss, Proctor & Brownjohn 2002).

The sharp transition between bright penumbral filaments and the almost featureless umbra apparently marks a critical combination of field strength and inclination. Penetration of bright filaments into the umbra is again likely to correspond to a traveling pattern rather than to bodily translation of flux tubes, although some interchanges may occur. Similarly, the difference in inclination between the fields

in bright and dark filaments must develop continuously at the umbral-penumbral boundary, and local interchanges between them are then possible in the neighborhood of this boundary.

5.3.2. INTERCHANGES IN THE DARK FILAMENTS The mode of convection in the dark filaments, whose inclination to the vertical increases with radius until they are almost horizontal at the edge of the spot, is clearly different and less effective. The most probable form of convection is in rolls whose axes lie in vertical planes containing the magnetic field, as originally suggested by Danielson (1961). These rolls are again confined to narrow slots, but now these slots can have only a limited vertical extent. Within them some form of interchange convection must take place, transferring energy not only upward but also radially inward from the external field-free plasma toward the center of the spot. There is a suggestion, from an extremely idealized asymptotic treatment of magnetoconvection in extremely narrow cells, that there is a sharp transition to a much less efficient mode of convection when the inclination of the field exceeds a critical value (Julien, Knobloch & Tobias 2000, 2003), but it is not known whether this result holds for models that are less constrained.

5.3.3. THIN FLUX TUBES IN THE PENUMBRA A different approach to penumbral convection was proposed by Schlichenmaier, Jahn & Schmidt (1998a,b; Schlichenmaier 2002). They considered the motion of a single isolated flux tube embedded within the axisymmetric global model of Jahn & Schmidt (1994). The flux tube starts at the magnetopause and its motion inward is triggered by impulsive heating from the external plasma. The intersection of this tube with the photosphere then moves inward as a bright point with an upflow (corresponding to a bright grain in the inner penumbra) while the outer portion of the tube, with an outflow, flops downward and may even dive beneath the photosphere (Schlichenmaier 2002). This is an instructive model, which illuminates some aspects of penumbral behavior, though it is not clear how it relates to the bright and dark filaments if their fields do remain distinct. A crucial difference between the flux tube model and the descriptions of convection presented above is that the isolated flux tube always retains its identity while neighboring fluid elements in a continuous fluid can drift arbitrarily far apart. (See also Section 3.3 for a general discussion of models of individual flux tubes.)

5.4. The Evershed Flow and Returning Penumbral Flux Tubes

The spectroscopic Evershed effect, consisting of a wavelength shift and asymmetry of spectral lines formed in the penumbra, is a prominent feature of all fully developed sunspots. Beginning with Evershed's (1909) discovery, this effect has been interpreted as a Doppler shift caused by a radial, nearly horizontal flow across the penumbra. The normal Evershed effect, in weak lines formed at photospheric heights, is consistent with a radial outflow of gas in the penumbra, while the reverse Evershed effect, seen in strong lines formed at chromospheric heights, is consistent

with an inflow into the umbra. Alternative interpretations invoking small-scale, unresolved wave motions have been proposed but are now considered untenable (see Thomas 1994 for a discussion).

5.4.1. FINE STRUCTURE OF THE EVERSHED FLOW Modern observations have shown that the photospheric Evershed flow is structured on fine scales and is time dependent. Beckers (1968) and Beckers & Schröter (1969) found the Evershed effect to be largely concentrated in the dark penumbral filaments. This association has been disputed (Wiehr & Stellmacher 1989, Lites, Skumanich & Scharmer 1990), but more recent high-resolution observations have generally confirmed at least a weak correlation between dark filaments and the Evershed flow (e.g., Title et al. 1993). The correlation is much stronger if intensity in the core of the spectral line (used to measure the Doppler velocity) is used instead of continuum intensity to define the dark filaments; in this case, the measurements of intensity and velocity are at more nearly the same height in the atmosphere (Rimmele 1995a, Stanchfield, Thomas, & Lites 1997). There is an even stronger correlation of the flow with the most nearly horizontal magnetic fields in the penumbra, as one would expect from magnetohydrodynamic considerations, which require that the flow be aligned with the magnetic field lines. Indeed, recent inversions of Stokes profiles based on a two-component model penumbral atmosphere (Bellot Rubio et al. 2003) produce magnetic fields and Evershed velocities that are well aligned everywhere across the penumbra.

Rimmele (1995a,b) found the Evershed flow to be confined to thin, loop-like channels elevated above the continuum level over much of the penumbra, and this configuration has been confirmed by subsequent observations (e.g., Stanchfield, Thomas & Lites 1997). Additionally, it has gradually been revealed that many of these elevated flow channels, with their associated magnetic fields, arch back down and actually dive below the surface at footpoints located in the outer penumbra or just outside the sunspot (Börner & Kneer 1992; Rimmele 1995b; Stanchfield, Thomas & Lites 1997; Westendorp Plaza et al. 1997, 2001; Schlichenmaier & Schmidt 1999, 2000; del Toro Iniesta, Bellot Rubio & Collados 2001; Bellot Rubio et al. 2002, 2003). The downflows at these footpoints can be supersonic (del Toro Iniesta, Bellot Rubio & Collados 2001).

The Evershed flow is time dependent, with the flow speeds along individual channels increasing and decreasing on timescales of 10–20 minutes (Shine et al. 1994, Rimmele 1994, Rouppe van der Voort 2003). This time dependence may be associated with changes in the gas pressure and magnetic field strength at the footpoints of the arched flux tube (Thomas 1994, Schlichenmaier, Jahn & Schmidt 1998b) or with movement of the flux tube vertically in and out of the range of heights of formation of the spectral line being observed (Rouppe van der Voort 2003). Outward-moving "clouds" of Evershed flow (Shine et al. 1994), originating in the inner penumbra, are coherent across several filaments and hence may be associated with some larger-scale wave motion rather than disturbances in individual Evershed flux tubes.

The observations of the Evershed effect are generally consistent with flows along many individual flux tubes in the penumbra. Some, perhaps most, of these flux tubes return below the solar surface near the outer penumbral boundary, while others continue radially outward along the elevated magnetic canopy. In either case, the configuration is consistent with the abrupt disappearance of the photospheric Evershed effect at the outer edge of a sunspot.

5.4.2. THEORETICAL MODELS OF THE EVERSHED FLOW The photospheric Evershed flow is generally treated as a flow along a thin magnetic flux tube driven by a pressure gradient along the tube (often called a "siphon flow": Meyer & Schmidt 1968). Models of steady-state flows along arched flux tubes, driven by a pressure drop between the two footpoints of the arch, reproduce the salient features of the observed flow, including the supersonic flow speeds in the descending part of the arch (Thomas and Montesinos 1993, Thomas 1996, Montesinos & Thomas 1997). In the case of supersonic flows, there is a "tube shock" somewhere along the descending leg of the arch where the flow abruptly becomes subsonic again and the gas pressure recovers to a typical photospheric value.

A typical Evershed flux tube emerges in the inner or middle penumbra and dives back below the surface in the outer penumbra or just beyond the outer penumbral boundary. For a thin magnetic flux tube in equilibrium, the total internal pressure (gas plus magnetic) balances the total pressure outside the tube. The pressure distribution outside the tube may be taken as fixed. The total internal pressure is the same at the two footpoints where an arched flux tube crosses a gravitational equipotential surface (on which the external pressure is constant). An outward flow along the tube is driven only when the gas pressure in the tube is lower at the outer footpoint than at the inner footpoint, which in turn requires that the magnetic pressure in the tube be higher at the outer footpoint than at the inner footpoint.[1] This is typically the case for a returning penumbral flux tube, for which the magnetic field strength at the inner footpoint is around 1000 G (a typical penumbral field strength) but at the outer footpoint is of order 1500 G (corresponding to a typical intense photospheric magnetic element).

A time-dependent model of the Evershed flow has been presented by Schlichenmaier, Jahn & Schmidt (1998a,b). In this model, a thin flux tube initially lies along the magnetopause (the outer edge of the sunspot's magnetic field) and extends outward to a point along the elevated magnetic canopy, where an open boundary condition is applied. The flux tube is heated in contact with the hotter surroundings, which causes the footpoint of the tube to move laterally inward (see

[1]This requirement applies just as well to transient flows, such as the quasi-steady serpentine flows computed by Schlichenmaier (2002), as to steady flows. We emphasize this, because statements to the contrary appear in the literature. Whether the pressure difference is produced by magnetic flux concentration at the downstream footpoint or by heating at the upstream footpoint, it is still a gradient in gas pressure that drives the flow, and the magnetic field strength will be higher at the outer footpoint in order to drive an outflow.

Section 3.3) while the resulting pressure increase drives a flow along the tube. In some cases with high flow velocities, cooling of the flow along elevated parts of the tube is strong enough to produce a local density increase sufficient to render the tube negatively buoyant, causing it to sink locally and producing a serpentine configuration for the flux tube and local downflows (Schlichenmaier 2002). (Such a sinusoidal configuration of the flux tube was found earlier for steady-state flows by Thomas & Montesinos 1990.) However, in this model all of the outflow continues along the magnetic canopy, but observations indicate that only small fraction of the flow does so. The sudden disappearance of most of the Evershed outflow near the boundary of the spot is explained if the flow is along returning flux tubes that are submerged outside the sunspot. These returning flux tubes, now well established by observations, raise an interesting theoretical question: what keeps them submerged in spite of their magnetic buoyancy? We discuss this in the next section.

6. FLUX PUMPING AND THE ORIGIN OF PENUMBRAL STRUCTURE

We have been led to a picture of penumbral structure involving two components, with different magnetic field inclinations, that remain essentially distinct from each other over the lifetime of the sunspot, with little interchange of magnetic flux (Figure 11). In the darker component, the magnetic field is nearly horizontal in the outer penumbra and in many places the inclination goes beyond 90° and the field dives back down below the surface, in the form of the returning flux tubes. What is the origin of this distinctive structure, and how is it maintained? What holds the submerged parts of the returning flux tubes down below the surface outside the sunspot, in opposition to the expected magnetic buoyancy force and curvature force on these tubes? Recently it has been proposed that downward pumping of magnetic flux by the turbulent granular convection provides the physical mechanism for this submergence (Thomas et al. 2002a,b; Weiss et al. 2004). This mechanism, sketched in Figure 11, helps to explain a number of other aspects of the penumbra, including its formation.

6.1. Turbulent Convective Pumping in the Moat

The idea of magnetic flux pumping traces back to earlier ideas of magnetic flux expulsion, turbulent diamagnetism, and topological pumping. However, in highly compressible, turbulent convection the dominant effect that leads to downward flux pumping is the asymmetry of the flow pattern consisting of strong, concentrated downdrafts and weaker, broad updrafts. This pumping has been shown to be important in the lower part of the solar convection zone, where it can transport magnetic flux into the underlying stable layers as part of the solar dynamo process (Tobias et al. 2001, Dorch & Nordlund 2001).

Flux pumping is also effective near the photosphere, because of the vigorous convection in the strongly superadiabatic granulation layer. Strong sinking

plumes in the granules and mesogranules in the moat can overcome both magnetic buoyancy and the effects of weaker upflows, and hence pump magnetic flux downward. Deeper down, below the granulation boundary layer, the more quiescent supergranular convection is far less effective at pumping magnetic flux downward, allowing flux to accumulate at the base of the granulation layer. The effectiveness of magnetic pumping by the granulation has been demonstrated in a series of three-dimensional numerical simulations of fully compressible convection (Thomas et al. 2002a,b; Weiss et al. 2004). Figure 12 shows results from one of these idealized experiments.

Such calculations certainly show that horizontal fields can be pumped downwards by turbulent small-scale convection. It still remains to be demonstrated that flux pumping is effective with the magnetic geometry of a sunspot, and that this mechanism is indeed able to drag the fields in dark filaments down below the photosphere. In addition to explaining the returning flux tubes, the flux pumping mechanism also helps explain the behavior of moving magnetic features in the moat surrounding a sunspot. Flux pumping may also play an important role in the formation and maintenance of the penumbra, as we next discuss.

6.2. Formation of the Penumbra

The development of an active region at the solar surface begins with the emergence of a rising, fragmented flux tube into the photosphere (Zwaan 1992). The magnetic field is initially confined to numerous small flux elements, which then accumulate at the boundaries between granules or mesogranules to form small pores (Keppens & Martínez Pillet 1996; Leka & Skumanich 1998). Dark pores are intense concentrations of magnetic flux that differ from sunspots in that they lack a penumbra. Pores have continuum intensities ranging from 80% down to 20% of the normal photospheric intensity, and maximum (central) magnetic field strength of 1500 to 2000 G. Magnetohydrostatic equilibrium of the pore's flux tube in the highly stratified photosphere requires that the magnetic field fan out with height, and indeed the observed inclination of the field to the local vertical typically varies from 0° at the center to about 35° at the outer edge of a pore. Doppler velocity measurements show the existence of an annular region of downflow immediately surrounding most pores (Keil et al. 1999, Tritschler, Schmidt & Rimmele 2002). These annuli have widths of 700–1500 km and flow speeds (measured in photospheric spectral lines) of order 300–500 m s^{-1}, and occasionally up to 1 km s^{-1}.

Sunspots form through the coalescence of pores and smaller magnetic flux tubes into a single, growing pore. The formation of a penumbra around the growing pore is a very rapid event; it occurs in less than twenty minutes, and the typical magnetic field geometry and Evershed flow are both established within this same short time (Leka & Skumanich 1998, Yang et al. 2003). This sudden change strongly suggests that the penumbra forms as a consequence of the onset of an instability of the magnetic field configuration in the growing pore. Simple equilibrium models already indicate that the inclination of the magnetic field at the edge of a pore

increases as the total magnetic flux increases and suggest that the configuration becomes unstable when this inclination reaches a critical value, at which point the pore develops a penumbra and becomes a sunspot (Simon & Weiss 1970; Rucklidge, Schmidt & Weiss 1995; Hurlburt & Rucklidge 2000). Observations indicate that the critical inclination angle (to the local vertical) is about 35°, which interestingly is the same as the inclination of the mean magnetic field at the umbra-penumbra boundary in a fully formed sunspot (Martínez Pillet 1997). There is apparently some hysteresis associated with the transition from a pore to a sunspot, because observations show that the largest pores are bigger than the smallest sunspots (Bray & Loughhead 1964, Rucklidge, Schmidt & Weiss 1995, Skumanich 1999).

The latest high-resolution observations reveal a narrow, finely fluted rim around the tiniest pores (Scharmer et al. 2002). In the absence of convection these magnetic configurations should be hydromagnetically stable, but small-scale convection within the umbra of a pore, combined with external granular convection, must excite the stable fluting modes to some small finite amplitude (Tildesley & Weiss 2004). It has been conjectured (Thomas et al. 2002a,b; Tildesley 2003; Weiss et al. 2004) that the flux tube of a growing pore does eventually become unstable to convectively driven filamentary perturbations, and that the nonlinear development of this instability leads to fluting at the outer boundary. This conjecture is supported both by detailed model calculations in an idealized Cartesian geometry (Tildesley 2003, Tildesley & Weiss 2004) and by some preliminary axisymmetric results (Hurlburt, Matthews, & Rucklidge 2000; Hurlburt & Alexander 2002). The resulting instability can produce the rudimentary penumbra seen in protospots (Leka & Skumanich 1998), but there is then a sudden jump associated with the appearance of a fully developed penumbra with its interlocking-comb magnetic field configuration. We conjecture that the depressed spokes in the mildly fluted field are eventually grabbed by sinking fluid in the surrounding granular convection and dragged downward, thus causing an abrupt transition to a new configuration with a fully developed penumbra. More realistic models are clearly needed to support this hypothesis. The flux pumping also keeps the magnetic field in dark filaments submerged as the sunspot decays, maintaining the penumbra even when the total magnetic flux becomes less than that of the pore from which the penumbra first formed. This hysteresis corresponds to the subcritical bifurcation proposed by Rucklidge, Schmidt & Weiss (1995).

7. OUTLOOK

The past decade has seen remarkable technical advances and improvements in the resolution of solar observations and in measurements of the vector magnetic field. We now have a fairly clear picture of sunspot structure and dynamics on a scale of $0.2''$ and we have glimpses of the structure at $0.1''$. The new picture of fine structure in a spot is complicated, with the interlocking-comb magnetic field, returning flux tubes, penumbral grains moving both inward and outward, etc., but for the first time

we are seeing the fundamental magnetoconvective and other dynamical processes in a sunspot.

Theory lags behind these observations. True, we are now able to put forward a broadly coherent physical picture of the key processes—convection, flux pumping, and siphon flows—that maintain the intricate structure of a spot's magnetic field. As yet, however, there are no detailed theoretical models that reproduce the features that have been observed. That must await further massive computation, facilitated by the development of ever more powerful processors. Meanwhile, observers will resolve yet finer details, and yet more powerful telescopes (the 1.5-m GREGOR and the 4-m ATST) will come on line. Helioseismology also offers the promise of revealing a sunspot's subsurface structure and the flows that help to maintain it (e.g., Zhao et al. 2001).

The Sun is a relatively inactive star. Whereas sunspots never cover more than about 0.1% of the solar surface, there are rapidly rotating late-type stars that are far more active, with dark spots occupying up to a quarter of their surfaces (Byrne 1992, Schrijver 2002). Moreover, Doppler imaging reveals that these spots are located preferentially at the poles. In their gross structure, these starspots are similar to sunspots. We have seen that the existence of the penumbra is a consequence of small-scale behavior, and it is only on the Sun that structures 100 km across will ever be resolved. Thus any detailed modeling of spots on magnetically active stars must rely on what we can learn from interpreting solar observations.

ACKNOWLEDGMENTS

We have benefited from discussions with a great many colleagues, and this review has been influenced by the information that they have supplied: to all, our thanks. We are especially grateful to Bruce Lites, Åke Nordlund, Thomas Rimmele, and Luc Rouppe van der Voort for providing figures before publication.

LITERATURE CITED

Acton DS, Smithson RC. 1992. *Appl. Opt.* 31: 3161–69

Antiochos S, et al. 1997. *The Solar-B Mission*. Rep. NASA Sci. Defin. Team

Balthasar H, Schleicher H, Bendlin C, Volkmer R. 1996. *Astron. Astrophys.* 315:603–9

Beckers JM. 1968. *Sol. Phys.* 3:258–68

Beckers JM, Schröter EH. 1969. *Sol. Phys.* 10:384–403

Bellot Rubio LR, Collados M, Ruiz Cobo B, Rodríquez Hidalgo I. 2002. *Nuovo Cim.* 25C:543–49

Bellot Rubio LR. 2003. See Trujillo-Bueno & Sánchez Almeida 2003, pp. 301–23

Bellot Rubio LR, Balthasar H, Collados M, Schlichenmaier R. 2003. *Astron. Astrophys.* 403:L47–50

Berger TE, Berdyugina SV. 2003. *Ap. J.* 589: L117–21

Blanchflower SM, Rucklidge AM, Weiss NO. 1998. *MNRAS* 301:593–608

Bonet JA, Ponz JD, Vázquez M. 1982. *Sol. Phys.* 77:69–75
Börner P, Kneer F. 1992. *Astron. Astrophys.* 259:307–12
Bray RJ, Loughhead RE. 1964. *Sunspots*. London: Chapman and Hall. 303 pp.
Byrne PB. 1992. See Thomas & Weiss 1992a, pp. 63–73
Cattaneo F. 1999. *Ap. J.* 515:L39–42
Cattaneo F, Emonet T, Weiss NO. 2003. *Ap. J.* 588:1183–98
Cowling TG. 1976. *MNRAS* 177:409–14
Cram LE, Thomas JH, eds. 1981. *The Physics of Sunspots*. Sunspot, NM: Sacramento Peak Obs. 495 pp.
Danielson RE. 1961. *Ap. J.* 134:289–311
Danielson RE. 1964. *Ap. J.* 139:45–47
Degenhardt D. 1989. *Astron. Astrophys.* 222: 297–306
Degenhardt D, Lites BW. 1993a. *Ap. J.* 404: 383–93
Degenhardt D, Lites BW. 1993b. *Ap. J.* 416: 875–85
Degenhardt D, Wiehr E. 1991. *Astron. Astrophys.* 252:821–26
del Toro Iniesta JC. 2003. *Astron. Nachr.* 324:383–87
del Toro Iniesta JC, Bellot Rubio LR, Collados M. 2001. *Ap. J.* 549:L139–42
del Toro Iniesta JC, Ruiz Cobo B. 1996. *Sol. Phys.* 164:169–82
Denker C. 1998. *Sol. Phys.* 180:81–108
Dorch SBF, Nordlund Å. 2001. *Astron. Astrophys.* 365:562–70
Evershed J. 1909. Radial movement in sunspots. *Kodaikanal Obs. Bull.* 15:63–69
Ewell MW Jr. 1992. *Sol. Phys.* 137:215–23
Fleck B, Keller CU. 2003. In *Dynamic Sun*, ed. BN Dwivedi, pp. 403–33. Cambridge, UK: Cambridge Univ. Press
Grossmann-Doerth U, Schmidt W, Schröter EH. 1986. *Astron. Astrophys.* 156:347–53
Hartkorn K, Rimmele T. 2003. See Pevtsov & Uitenbroek 2003, pp. 281–90
Hofmann J, Deubner F-L, Fleck B, Schmidt W. 1994. *Astron. Astrophys.* 284:269–75
Hurlburt N, Alexander D. 2002. In *COSPAR Colloquia Ser. 14: Solar-Terrestrial Magnetic Activity and Space Environment*, ed. H Wang, R Xu, pp. 19–25. Oxford, UK: Pergamon
Hurlburt NE, Matthews PC, Proctor MRE. 1996. *Ap. J.* 457:933–38
Hurlburt NE, Matthews PC, Rucklidge AM. 2000. *Sol. Phys.* 192:109–18
Hurlburt NE, Rucklidge AM. 2000. *MNRAS* 314:793–806
Jahn K. 1992. See Thomas & Weiss 1992a, pp. 139–62
Jahn K. 1997. See Schmieder, del Toro Iniesta & Vázquez 1997. pp. 122–39
Jahn K, Schmidt HU. 1994. *Astron. Astrophys.* 290:295–317
Julien K, Knobloch E, Tobias SM. 2000. *J. Fluid Mech.* 410:285–322
Julien K, Knobloch E, Tobias SM. 2003. In *The Fluid Mechanics of Astrophysics and Geophysics Vol. 9: Advances in Nonlinear Dynamos*, ed. A Ferriz-Mas, M Núñez-Jimenez, pp. 195–223. Bristol, UK: Taylor & Francis
Keil SL, Balasubramaniam KS, Smaldone LA, Reger B. 1999. *Ap. J.* 510:422–43
Keller CU. 1999. See See Rimmele, Balasubramaniam & Radick 1999, pp. 169–76
Keller CU. 2003. See Pevtsov & Uitenbroek 2003, pp. 31–44
Keppens R, Martínez Pillet V. 1996. *Astron. Astrophys.* 316:229–42
Kitai R. 1986. *Sol. Phys.* 104:287–301
Kneer F. 1973. *Sol. Phys.* 28:361–67
Kneer F, Soltau D, Wiehr E. 1990. In *IAU Symp. 142: Basic Plasma Processes in the Sun*, ed. ER Priest, V Krishnan, pp. 113–17. Dordrecht: Kluwer
Knox KT, Thompson BJ. 1974. *Ap. J.* 193:L45–48
Leka KD. 1997. *Ap. J.* 484:900–19
Leka KD, Skumanich A. 1998. *Ap. J.* 507:454–69
Lites BW, Bida TA, Johannesson A, Scharmer GB. 1991. *Ap. J.* 373:683–94
Lites BW, Elmore DF, Seagraves P, Skumanich AP. 1993. *Ap. J.* 418:928–42
Lites BW, Elmore DF, Streander KV, Sankarasubramanian K, Rimmele TR, Sigwarth

M. 2003. See Trujillo-Bueno & Sánchez Almeida 2003, pp. 324–29

Lites BW, Scharmer GB, Berger TE, Title AM. 2004. *Sol. Phys.* In press

Lites BW, Skumanich A, Scharmer GB. 1990. *Ap. J.* 355:329–41

Martínez Pillet V. 1997. See Schmieder, del Toro Iniesta & Vázquez 1997, pp. 212–36

Martínez Pillet V, Collados M, Sánchez Almeida J, González V, Cruz-Lopez A, et al. 1999. See Rimmele, Balasubramaniam & Radick 1999, pp. 264–72

Martínez Pillet V, Sobotka M, Vázquez M, Shine RA. 2003. Preprint

Mathew SK, Solanki SK, Lagg A, Collados M, Berdyugina SV, et al. 2003 *Astron. Nachr.* 324:388–89

Matthews PC, Hurlburt NE, Proctor MRE, et al. 1992. *J. Fluid Mech.* 240:559–69

Meyer F, Schmidt HU. 1968. *Zeits. Ang. Math. Mech.* 48:T218–21

Molowny-Horas R. 1994. *Sol. Phys.* 154:29–39

Montesinos B, Thomas JH. 1997. *Nature* 390: 485–87

Muller R. 1973a. *Sol. Phys.* 29:55–73

Muller R. 1973b. *Sol. Phys.* 32:409–20

Pahlke K-D, Wiehr E. 1990. *Astron. Astrophys.* 228:246–52

Paxman RG, Seldin JH, Keller CU. 1999. See Rimmele, Balasubramaniam & Radick 1999, pp. 311–19

Pevtsov AA, Uitenbroek H, eds. 2003. *ASP Conf. Ser. 286: Current Theoretical Models and High Resolution Solar Observations: Preparing for ATST*. San Francisco: Astron. Soc. Pac. 452 pp.

Proctor MRE. 1992. See Thomas & Weiss 1992a, pp. 221–41

Rimmele TR. 1994. *Astron. Astrophys.* 290: 972–82

Rimmele TR. 1995a. *Astron. Astrophys.* 298: 260–76

Rimmele TR. 1995b. *Ap. J.* 445:511–16

Rimmele TR. 1997. *Ap. J.* 490:458–69

Rimmele TR. 2004. *Ap. J.* 606:906–23

Rimmele TR, Balasubramaniam KS, Radick RR, eds. 1999. *ASP Conf. Ser. 183: High Resolution Solar Physics: Theory, Observations, and Techniques*. San Francisco: Astron. Soc. Pac. 568 pp.

Rimmele TR, Keil SL, Keller C, Hill F, Penn M, et al. 2003. See Pevtsov & Uitenbroek 2003, pp. 3–22

Rimmele TR, Radick RR. 1998. *Proc. SPIE* 3353:72–81

Rouppe van der Voort LHM. 2003. *Astron. Astrophys.* 397:757–64

Rouppe van der Voort LHM, Löfdahl MG, Kiselman D, Scharmer GB. 2004. *Astron. Astrophys.* 414:717–26

Rucklidge AM, Schmidt HU, Weiss NO. 1995. *MNRAS* 273:491–98

Rucklidge AM, Weiss NO, Brownjohn DP, et al. 2000. *J. Fluid Mech.* 419::283–323

Sams BJ, Golub L, Weiss NO. 1992. *Ap. J.* 399:313–17

Sánchez Almeida J, Bonet JA. 1998. *Ap. J.* 505:1010–17

Scharmer GB, Owner-Petersen M, Korhonen T, Title A. 1999. See Rimmele, Balasubramaniam & Radick 1999, pp. 157–68

Scharmer GB, Gudiksen BV, Kiselman D, Löfdahl MG, Rouppe van der Voort LHM. 2002. *Nature* 420:151–53

Schlichenmaier R. 2002. *Astron. Nachr.* 323: 303–8

Schlichenmaier R, Jahn K, Schmidt HU. 1998a. *Ap. J.* 493:L121–24

Schlichenmaier R, Jahn K, Schmidt HU. 1998b. *Astron. Astrophys.* 337:897–910

Schlichenmaier R, Schmidt W. 1999. *Astron. Astrophys.* 349:L37–40

Schlichenmaier R, Schmidt W. 2000. *Astron. Astrophys.* 358:1122–32

Schlüter A, Temesváry S. 1958. In *IAU Symp. No. 6: Electromagnetic Phenomena in Cosmical Physics*, ed. B Lehnert, pp. 263–71. Cambridge, UK: Cambridge Univ. Press

Schmidt HU. 1991. *Geophys. Astrophys. Fluid Dyn.* 62:249–70

Schmidt W, Balthasar H. 1994. *Astron. Astrophys.* 283:241–46

Schmidt W, Hofmann A, Balthasar H, Tarbell TD, Frank ZA. 1992. *Astron. Astrophys.* 264:L27–30

Schmieder B, del Toro Iniesta JC, Vázquez M,

eds. 1997. *ASP Conf. Ser. 118: Advances in the Physics of Sunspots*. San Francisco: Astron. Soc. Pac. 418 pp.
Schrijver C. 2002. *Astron. Nachr.* 323:157–64
Schüssler M. 2001. See Sigwarth 2001, pp. 343–54
Shine RA, Title AM, Tarbell TD, Smith K, Frank ZA, Scharmer G. 1994. *Ap. J.* 430:413–24
Sigwarth M, ed. 2001. *ASP Conf. Ser. 236: Advanced Solar Polarimetry—Theory, Observation, and Instrumentation*. San Francisco: Astron. Soc. Pac. 615 pp.
Simon GW, Weiss NO. 1970. *Sol. Phys.* 13:85–103
Skumanich A. 1999. *Ap. J.* 512:975–84
Sobotka M, Bonet JA, Vázquez M. 1993. *Ap. J.* 415:832–46
Sobotka M, Brandt PN, Simon GW. 1997a. *Astron. Astrophys.* 328:682–88
Sobotka M, Brandt PN, Simon GW. 1997b. *Astron. Astrophys.* 328:689–94
Sobotka M, Brandt PN, Simon GW. 1999. *Astron. Astrophys.* 348:621–26
Sobotka M, Muller R, Bonet JA, Márquez I. 2002. In *Magnetic Coupling of the Solar Atmosphere*, ESA SP-505, ed. H Sawaya-Lacoste, pp. 579–82. Noordwijk, Neth.: ESA Publ. Div.
Sobotka M, Sütterlin P. 2001. *Astron. Astrophys.* 380:714–18
Socas-Navarro H. 2001. See Sigwarth 2001, pp. 487–501
Socas-Navarro H. 2003. See Pevtsov & Uitenbroek 2003, pp. 267–80
Solanki SK. 2003. *Astron. Astrophys.* 11:153–286
Solanki SK, Gandorfer AM, Schüssler M, Curdt W, Lites BW, Martínez Pillet V, Schmidt W, Title AM. 2003. *Proc. SPIE* 4853:129–39
Solanki SK, Montavon CAP. 1993. *Astron. Astrophys.* 275:283–92
Spruit HC. 1992. See Thomas & Weiss 1992a, pp. 163–71
Stanchfield DCH II, Thomas JH, Lites BW. 1997. *Ap. J.* 477:485–94
Stein RF, Nordlund Å. 1998. *Ap. J.* 499:914–33
Stenflo J. 1994. *Solar Magnetic Fields*. Dordrecht: Kluwer. 385 pp.
Stix M. 2002. *The Sun*. Berlin: Springer. 490 pp. 2nd ed.
Sütterlin P. 2001. *Astron. Astrophys.* 374:L21–24
Thiessen G. 1950. *Observatory* 70:234–35
Thomas JH. 1988. *Ap. J.* 333:407–19
Thomas JH. 1994. In *Solar Surface Magnetism*, ed. RJ Rutten, CJ Schrijver, pp. 219–35. Dordrecht: Kluwer
Thomas JH. 1996. In *Solar and Astrophysical Magnetohydrodynamic Flows*, ed. KC Tsinganos, pp. 39–60. Dordrecht: Kluwer
Thomas JH. 1999. See Rimmele, Balasubramaniam & Radick 1999, pp. 1–16
Thomas JH, Montesinos B. 1990. *Ap. J.* 359: 550–59
Thomas JH, Montesinos B. 1993. *Ap. J.* 407: 398–401
Thomas JH, Weiss NO, eds. 1992a. *Sunspots: Theory and Observations*. Dordrecht: Kluwer. 428 pp.
Thomas JH, Weiss NO. 1992b. See Thomas & Weiss 1992a, pp. 3–59
Thomas JH, Weiss NO, Tobias SM, Brummell NH. 2002a. *Nature* 420:390–93
Thomas JH, Weiss NO, Tobias SM, Brummell NH. 2002b. *Astron. Nachr.* 323:383–86
Tildesley MJ. 2003. *MNRAS* 338:497–507
Tildesley MJ, Weiss NO. 2004. *MNRAS* 350:657–70
Title A, Frank ZA, Shine RA, Tarbell TD, Topka KP, Scharmer G, Schmidt W. 1992. See Thomas & Weiss 1992a, pp. 195–219
Title A, Frank ZA, Shine RA, Tarbell TD, Topka KP, Scharmer G, Schmidt W. 1993. *Ap. J.* 403:780–96
Tobias SM, Brummell NH, Clune TL, Toomre J. 2001. *Ap. J.* 549:1183–203
Tönjes K, Wöhl H. 1982. *Sol. Phys.* 75:63–69
Tritschler A, Schmidt W. 1997. *Astron. Astrophys.* 321:643–51
Tritschler A, Schmidt W. 2002a. *Astron. Astrophys.* 382:1093–105
Tritschler A, Schmidt W. 2002b. *Astron. Astrophys.* 388:1048–61
Tritschler A, Schmidt W, Rimmele T. 2002. In

Proc. 10th Eur. Solar Physics Meet., Solar Variability: From Core to Outer Frontiers, ESA SP-506, pp. 477–78

Trujillo-Bueno J, Sánchez Almeida J, eds. 2003. *ASP Conf. Ser. 307: Solar Polarization Workshop 3*. San Francisco: Astron. Soc. Pac. 615 pp.

Vázquez M. 1973. *Sol. Phys.* 31:377–87

Vögler A, Schüssler M. 2003. *Astron. Nachr.* 324:399–404

von der Lühe O. 1983. *Astron. Astrophys.* 119:85–94

Wang H, Zirin H. 1992. *Sol. Phys.* 140:41–54

Weiss NO. 2002. *Astron. Nachr.* 323:371–76

Weiss NO, Brownjohn DP, Hurlburt NE, Proctor MRE. 1990. *MNRAS* 245:434–52

Weiss NO, Brownjohn DP, Matthews PC, Proctor MRE. 1996. *MNRAS* 283:1153–64

Weiss NO, Proctor MRE, Brownjohn DP. 2002. *MNRAS* 337:293–304

Weiss NO, Thomas JH, Brummell NH, Tobias SM. 2004. *Ap. J.* 600:1073–90

Westendorp Plaza C, del Toro Iniesta JC, Ruiz Cobo B, Martínez Pillet V, Lites BW, Skumanich A. 1997. *Nature* 389:47–49

Westendorp Plaza C, del Toro Iniesta JC, Ruiz Cobo B, Martínez Pillet V. 2001. *Ap. J.* 547:1148–58

Wiehr E. 1994. *Astron. Astrophys.* 287:L1–4

Wiehr E, Degenhardt D. 1993. *Astron. Astrophys.* 278:584–88

Wiehr E, Stellmacher G. 1989. *Astron. Astrophys.* 225:528–32

Winebarger AR, DeLuca EE, Golub L. 2001. *Ap. J.* 553:L81–84

Winebarger AR, Warren H, van Ballegooijen A, DeLuca EE, Golub L. 2002. *Ap. J.* 567:L89–92

Yang G, Xu Y, Wang H, Denker C. 2003. *Ap. J.* 597:1190–99

Zhao J, Kosovichev AG, Duvall TL Jr. 2001. *Ap. J.* 557:384–88

Zwaan C. 1992. See Thomas & Weiss 1992a, pp. 75–100

Zwaan C, Brants JJ, Cram LE. 1985. *Sol. Phys.* 95:3–14

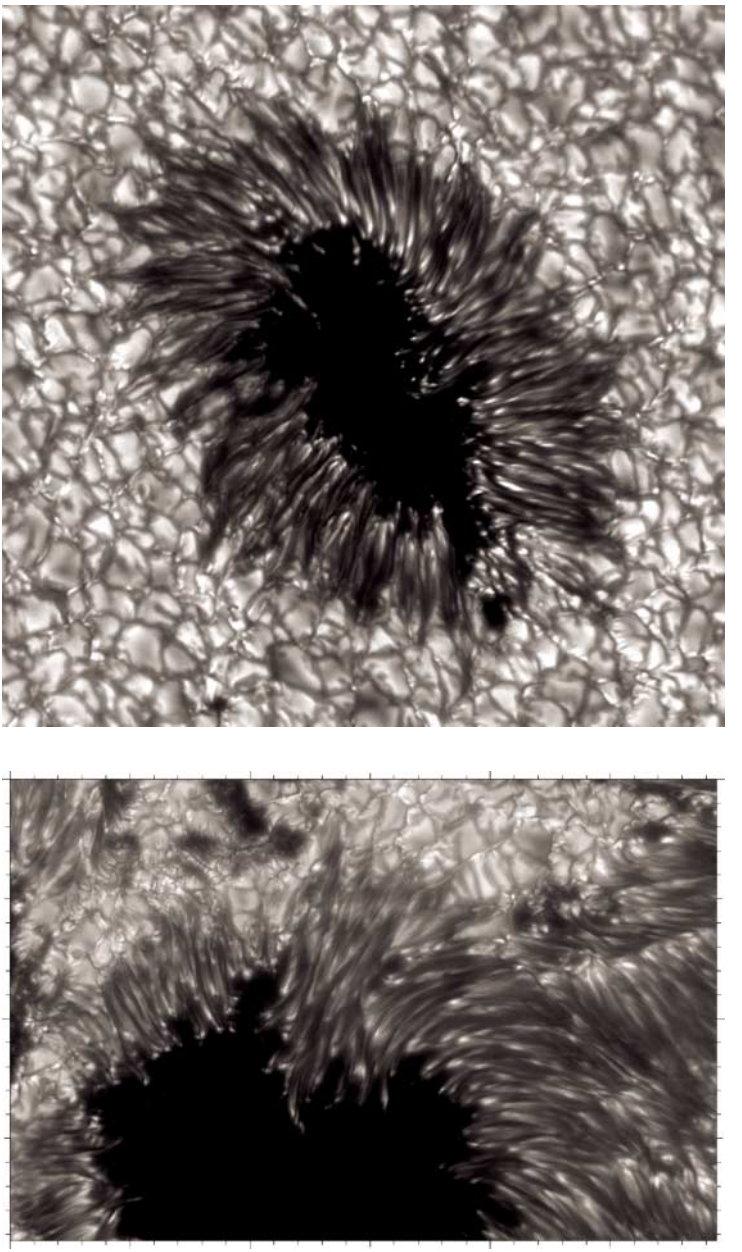

Figure 1 Swedish 1-m Solar Telescope images showing fine structure in two different sunspots, each near disk center. (*Top*) Continuum image near 436 nm (courtesy of L. Rouppe van der Voort, University of Oslo). (*Bottom*) G-band image at 430.5 nm (from Scharmer et al. 2002). Tick marks have a spacing of 1000 km on the Sun.

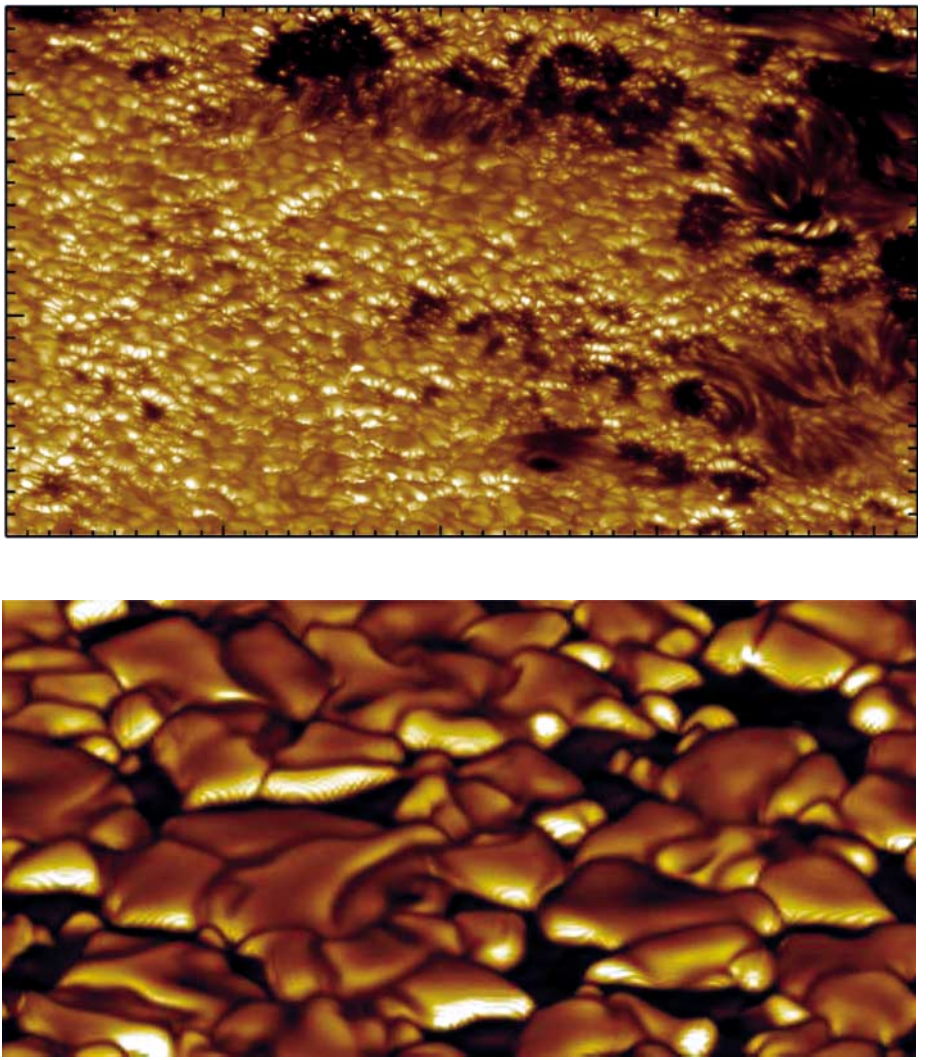

Figure 2 (*Top*) Image of an active region near the solar limb taken with the Swedish 1-m Solar Telescope, in an 8-nm bandpass centered at 487.7 nm. Tick marks have a spacing of 1″ (720 km on the Sun). This image gives a perspective view of the three-dimensional structure of photospheric features in sunspots, pores, and granulation (from Lites et al. 2004). (*Bottom*) Image of the emergent intensity, as viewed from 60° inclination to the vertical, based on a realistic numerical simulation of a facular region, for comparison with the observed structure in the image above (but note the different spatial scale) (courtesy of Å. Nordlund).

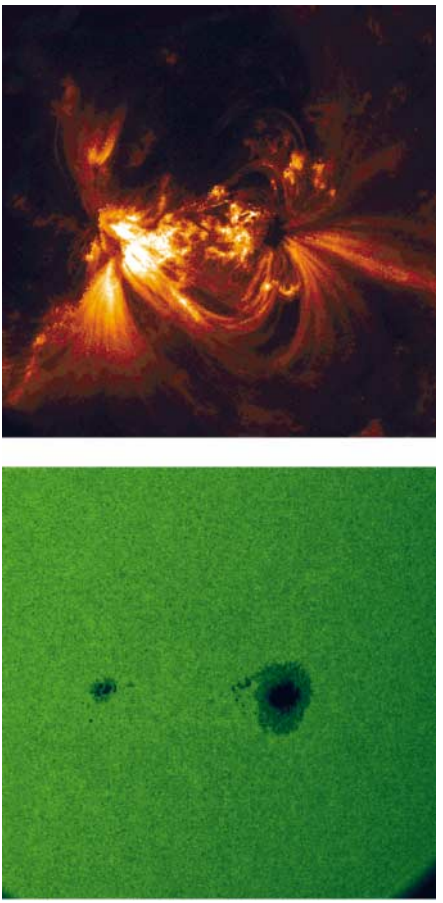

Figure 4 TRACE image of coronal loops connecting two sunspots and a white-light image of the same region. Such images show that magnetic loops emerging from bright penumbral filaments often extend over great distances on the Sun, implying that the magnetic fields in bright and dark filaments remain essentially distinct over the lifetime of a sunspot (courtesy of the Lockheed Martin Solar and Astrophysics Laboratory).

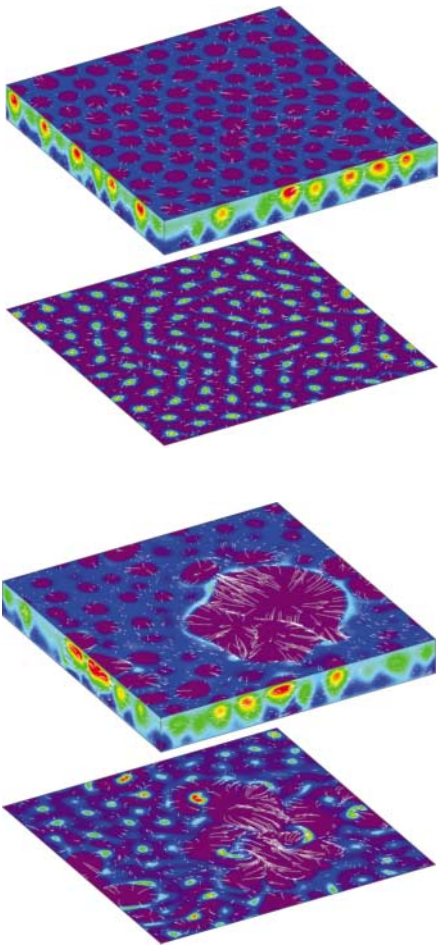

Figure 5 Three-dimensional magnetoconvection in a strong magnetic field. The upper panel shows small-scale spatially modulated oscillations, with magnetic flux swept aside by the rising plumes and confined to a network at the top of the layer. The lower panel, for the same parameter values, shows a flux-separated solution, with a cluster of broad and vigorous plumes from which magnetic flux has been expelled, surrounded by small-scale convection. The images show the variation of magnetic energy density across the top and (reflected) the bottom of the layer; temperature fluctuations are indicated on the sides of the periodic box and arrows represent the tangential velocity. The color table runs through the spectrum from red (strong fields, hot fluid) to violet (weak fields, cold fluid) (after Weiss, Proctor & Brownjohn 2002).

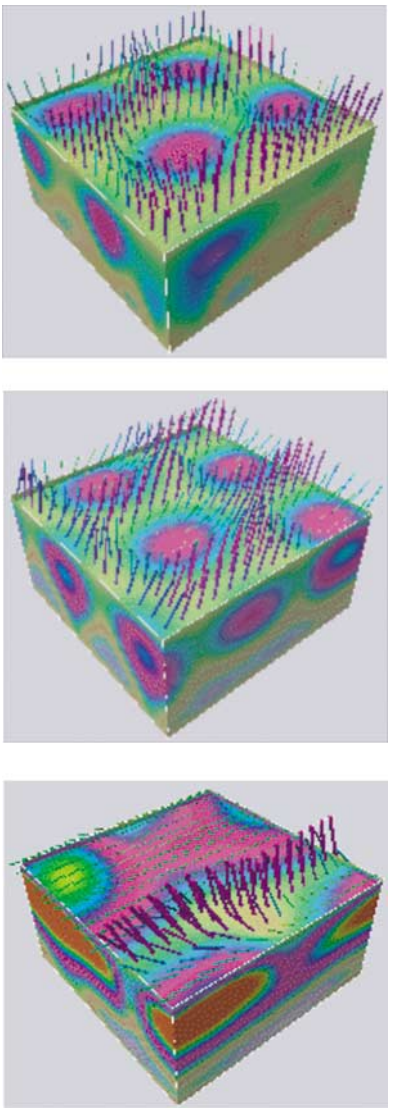

Figure 6 Small-scale magnetoconvection in fields inclined at an angle ϕ to the vertical. The three cases show (from top to bottom) spatially modulated oscillations for $\phi = 0°$, a modulated traveling wave for $\phi = 22°$, and an almost roll-like modulated traveling wave for $\phi = 67°$. The patterns travel away from the direction of tilt. The color scale shows temperature fluctuations at or near the walls of the box. Violet and yellow regions denote hot and cold fluid, respectively. The rods represent the strength and direction of the surface field (after Hurlburt, Matthews & Rucklidge 2000).

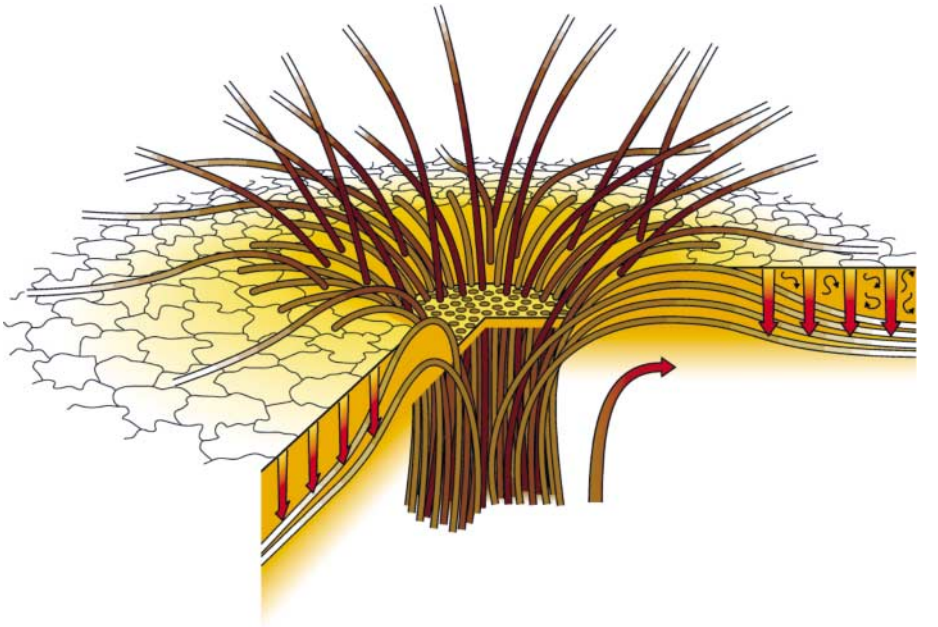

Figure 11 Sketch showing the interlocking-comb structure of the magnetic field in the filamentary penumbra of a sunspot (after Thomas et al. 2002a). The bright radial filaments, where the magnetic field is inclined (at approximately 40° to the horizontal in the outer penumbra), alternate with dark filaments in which the field is nearly horizontal. Within the dark filaments, some magnetic flux tubes (i.e., bundles of magnetic field lines) extend radially outward beyond the penumbra along an elevated magnetic canopy, while other, "returning" flux tubes dive back below the surface. The sunspot is surrounded by a layer of small-scale granular convection (*squiggly arrows*) embedded in the radial outflow associated with a long-lived annular supergranule (the moat cell) (*large curved arrow*). The submerged parts of the returning flux tubes are held down by turbulent pumping (*vertical arrows*) by the granular convection in the moat.

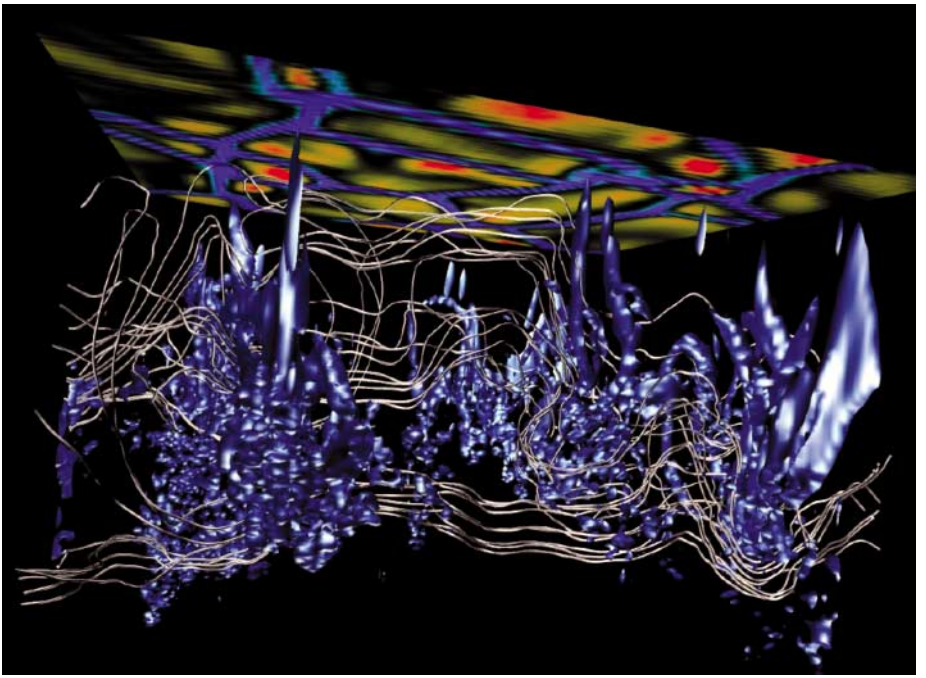

Figure 12 Downward magnetic flux pumping by vigorous sinking plumes in a simulation of granular convection (from Thomas et al. 2002a). At the top of this perspective view (from below the surface) is a two-dimensional representation of the vertical velocity just below the surface, showing a network of downflows (*light blue/blue*) surrounding broad upflows (*yellow/red*). The strong descending plumes are outlined by the illuminated surfaces (*in blue*) of constant enstrophy density (i.e., vorticity squared). The magnetic field is visualized by tracing selected bundles of magnetic field lines, some in the upper granulation layer and others pumped down into in nearly adiabatic layer below.

Annual Review of Astronomy and Astrophysics
Volume 42, 2004

CONTENTS